Reassessing the variability in atmospheric H_2 using the two-way nested TM5 model

G. Pieterse[1], M. C. Krol[1,2], A. M. Batenburg[1], C. A. M. Brenninkmeijer[3], M. E. Popa[1,7], S. O'Doherty[4], A. Grant[4], L. P. Steele[5], P. B. Krummel[5], R. L. Langenfelds[5], H. J. Wang[6], A. T. Vermeulen[7], M. Schmidt[8], C. Yver[8], A. Jordan[9], A. Engel[10], R. E. Fisher[11], D. Lowry[11], E. G. Nisbet[11], S. Reimann[12], M. K. Vollmer[12], M. Steinbacher[12], S. Hammer[13], G. Forster[14], W. T. Sturges[14], and T. Röckmann[1]

G. Pieterse, Institute for Marine and Atmospheric Research Utrecht (IMAU), Princetonplein 5, 3584 CC, Utrecht, The Netherlands. (Gerben_Pieterse@hotmail.com)

[1]Institute for Marine and Atmospheric

Abstract. This work reassesses the global atmospheric budget for molecular hydrogen (H_2) and its singly deuterated isotopologue HD by means of the two-way nested TM5 model. A recent adjustment of the calibration scale for H_2 measurements translates into a change in the tropospheric burden. Furthermore, the ERA Interim reanalysis data from the European Centre for Medium-Range Weather Forecasts used for this study shows slower vertical transport than the operational data used before. As a result, more H_2 is removed by dry deposition. Because our previous dry deposition parametrisation allowed for small but significant deposition of H_2 to snow and water surfaces, wetted surfaces and vegetation, the deposition parametrisation is updated. It is shown that the assumed timescales for the transport of H_2 through vegetation canopies are critical for obtaining realistic deposition fluxes to soils in vegetated regions. The best agreement between the modelled H_2 mixing ratios and isotopic compositions with new measurements from a European observation network and a global flask sampling network is obtained by asserting typical timescales of 1–2 hours for densely vegetated regions. Despite this adjustment, the H_2 mixing ratios are still slightly overestimated for the SH because too little H_2 is removed by dry deposition to rainforest and Savannah ecosystems. The regional scale variability in H_2 over Europe is further investigated using a high res-

Research Utrecht (IMAU), Utrecht, The

olution zoom over Europe. The analysis supports the conclusion from the global scale analysis and shows that remaining discrepancies can be largely attributed to representativeness effects due to the limited model resolution. The new tropospheric burden derived by the model is 165 Tg H_2. The removal rates of H_2 by deposition and photochemical oxidation are estimated at 53 and 23 Tg H_2/yr, resulting in a tropospheric lifetime of 2.2 yr for H_2.

Netherlands

1. Introduction

Since the industrialisation of fuel cell technology during the 1970s and 80s, molecular hydrogen (H_2) has been considered as a clean alternative for fossil fuel based energy carriers. The selective oxidation of H_2 by oxygen only produces water, contrary to the combustion of fossil fuels with air that produces carbon dioxide, carbon monoxide, nitrogen oxides, soot, and many other volatile organic compounds. As H_2 is not readily available in large quantities, practical applications of fuel cell technology rely on conversion from other energy carriers (*e.g.* bio fuels or fossil fuels) or generation of H_2 from direct energy sources (*e.g.* solar energy). The low overall well-to-wheel efficiency of the entire energy production chain and the accompanying costs, have so far limited the use of H_2 to a relatively small number of applications. Nevertheless, the potential for improving urban air quality and reducing the human impact on climate remains appealing. The ~~above-mentioned~~ positive effects of ~~its~~**H_2** usage on air quality and climate might be accompanied by adverse effects. Scaling up the use of H_2 might lead to an increasing input of H_2 into the atmosphere and, thus, to a larger atmospheric burden of H_2. Enhanced levels of H_2 might prolong the atmospheric life time of the greenhouse gas methane and **increase** its effect on climate [Schultz *et al.*, 2003]. Like methane, H_2 is removed from the atmosphere ~~by~~**via** chemical oxidation ~~with~~**by** the hydroxyl (OH) radical. Higher levels of H_2 ~~will lead to a larger consumption of~~**would consume more** OH radicals and herewith reduce the photochemical destruction of CH_4. ~~Because~~**As** the oxidation of H_2 produces

---

[2]Department of Meteorology and Air

water [Tromp *et al.*, 2003; Warwick *et al.*, 2004; Feck *et al.*, 2008], increasing H_2 mixing ratios in the stratosphere might also enhance the formation of polar stratospheric clouds. This in turn can result in increased chlorine activation and subsequent loss of ozone **during the polar spring**, although the effect is probably small in view of the variability of stratospheric water vapour [Vogel *et al.*, 2012].

A good understanding of the present day global H_2 cycle is a prerequisite to anticipate any adverse effects as a result of additional H_2 emissions that can be expected from a more intensified use as energy carrier. Observations of atmospheric H_2 mixing ratios were only scarcely available until the Global Monitoring Division (GMD), nowadays the Earth System Research Laboratory (ESRL), ~~of~~**at** the National Oceanic and Atmospheric Administration (NOAA) started systematic flask measurements at five sites in 1989 increasing to ~~up to~~ 52 sites during the 1990s. Additional data has been generated for 11 sites since the early 1990s by the Commonwealth Scientific and Industrial Research Organisation [CSIRO: Francey *et al.*, 1996; Langenfelds *et al.*, 2002; Jordan and Steinberg, 2011]. The results from the NOAA/ESRL network ~~esults~~ have been analysed extensively by Novelli *et al.* [1999] and translated to a global budget. ~~It is now established that~~ H_2 is emitted into the atmosphere due to the usage of fossil fuels, by biomass burning and as a reaction product of nitrogen fixation processes in the soils and oceans. Furthermore, it is photochemically produced from CH_4 and non-methane hydrocarbons (NMHCs). H_2 is removed from the atmosphere by photochemical **reaction** with OH and by dry deposition to the soils. The values of the magnitudes of the sources and sinks reported by Novelli *et al.* [1999] are still supported by most recent studies but the uncertainties remain large

Quality at Wageningen University,

[Hauglustaine and Ehhalt, 2002; Sanderson *et al.*, 2003; Rhee *et al.*, 2006; Price *et al.*, 2007; Xiao *et al.*, 2007; Ehhalt and Rohrer, 2009; Pison *et al.*, 2009; Yver *et al.*, 2011; Bousquet *et al.*, 2011; Pieterse *et al.*, 2011; Yashiro *et al.*, 2011]. Two of these studies [Rhee *et al.*, 2006; Xiao *et al.*, 2007] report a significantly larger contribution of the main sink of H_2, *i.e.* dry deposition, to the global budget than all others. ~~Ehhalt and Rohrer (2009) have proposed that the magnitude of the soil sink might indeed be overestimated by these studies because to balance the atmospheric burden, such large deposition fluxes would need a photochemical source magnitude for the production of H_2 from CH_4 and the NMHCs that is incompatible with the atmospheric budget of carbon monoxide (CO). Exclusion of these estimates would significantly reduce the overall reported range of uncertainty for the photochemical production and removal by deposition, providing a more unified view on the present day global budget of H_2.~~

In a number of the above mentioned studies, three-dimensional chemical transport models (CTMs) were used to study the global and regional H_2 cycles [Hauglustaine and Ehhalt, 2002; Sanderson *et al.*, 2003; Yashiro *et al.*, 2011] by means of comparison with available measurements of H_2 mixing ratios. Pison *et al.* [2009], Yver *et al.* [2011] and Bousquet *et al.* [2011] used ~~the~~**atmospheric** observations of H_2 mixing ratios and other species to determine the magnitudes of the source and sink processes by means of a Bayesian inverse modelling approach adopted from Bousquet *et al.* [2005]. In order to further constrain the global H_2 budget, Price *et al.* [2007] implemented the sources and sinks for the singly-deuterated stable H_2 isotopologue (HD) assuming a fixed ratio between the photochemical production of H_2 and HD. Modelled and measured isotopic compositions

Wageningen, The Netherlands

of molecular hydrogen are all calculated from the ~~per atom basis~~ ratio $R = D/H$ as $\delta D\,[H_2] = (R/R_{VSMOW} - 1)$, where $R_{VSMOW} = 1.558 \times 10^{-4}$ is the reference D/H ratio of Vienna Standard Mean Ocean Water (VSMOW). The resulting framework was also used to evaluate the stable H_2 isotope budgets previously reported by Gerst and Quay [2001]; Rahn *et al.* [2002, 2003]; Rhee *et al.* [2006]. A full H_2 isotope chemistry scheme was recently implemented in the TM5 model [Pieterse *et al.*, 2009, 2011] and used to further constrain the global budget of H_2 with $\delta D\,[H_2]$ measurements. Both studies showed that the modelled tropospheric $\delta D\,[H_2]$ is very sensitive to the values of the isotopic composition of stratospheric molecular hydrogen that is heavily enriched with deuterium [Rahn *et al.*, 2003; Röckmann *et al.*, 2003]. This sensitivity suggests an important role of the stratosphere troposphere exchange (STE) ~~in~~**for** the tropospheric HD budget and stresses the importance of using an appropriate stratospheric chemistry scheme or correct boundary condition.

The objective of this study is to further constrain the global H_2 budget by ~~adjusting the individual source and/or sink magnitudes to match the~~**comparing** model results ~~with the~~**to** measured H_2 mixing ratios and isotopic compositions, and by using the ratio between photochemical production of H_2 and CO as an additional constraint. For ~~this purpose~~**the first time**, we compare our model results to **high temporal resolution H_2** measurements from the EuroHydros project [Engel and EUROHYDROS PIs, 2009]. ~~This network was funded by the Sixth Framework program of the European Commission between 2006 and 2009 to set up a network of 12 stations with continuous H_2 observations~~

---

[3]Max-Planck-Institut für Chemie, Air

~~distributed over Europe.~~ The hourly H_2 mixing ratios measured at ~~a subset of~~ these stations are used to evaluate the modelled H_2 mixing ratios. Additionally, the **values of** $\delta D\,[H_2]$ ~~of~~**in** air collected at 5 flask sampling sites during the EuroHydros project [Batenburg *et al.*, 2011] are used to evaluate the model~~ed isotopic compositions~~ **results**. ~~An additional~~**A further** constraint is provided by the isotopic compositions of air samples collected **in the upper troposphere and the lower stratosphere** by the CARIBIC (Civil Aircraft for the Regular Investigation of the Atmosphere Based on an Instrument Container) program [Brenninkmeijer *et al.*, 2007; Batenburg *et al.*, 2012].~~The isotopic compositions of these samples, that were collected at cruise altitude (between 9 and 11 km) and analysed offline by isotope ratio mass spectrometry, are representative for the upper troposphere and the lower stratosphere.~~

The required changes to match the TM5 model results with the new observations are described in Section 2, along with the recent update of the calibration scale for H_2 measurements [Jordan and Steinberg, 2011] adopted by the World Meteorological Organisation (WMO). Section 3 starts with an evaluation of modelled global and latitudinal variability in H_2 and $\delta D\,[H_2]$ **in Section 3.1 and Section 3.2, respectively. Subsequently, the regional scale model performance is evaluated in Section 3.3 by means of a wind sector analysis for a selection of stations from the EuroHydros project** ~~**and by a detailed analysis of the temporal evolution of the modelled and measured H_2 and CO mixing ratios at Mace Head**~~**. Section 4 proceeds by discussing the implications of the study for the global H_2 budget and the overall conclusions are summarised in Section 5.**

Chemistry Division, Mainz, Germany

2. Methods

The two-way nested setup of the TM5 model [Krol *et al.*, 2005] was recently enhanced by implementing a H_2 isotope chemistry scheme [Pieterse *et al.*, 2009], **an H_2 emission inventory adopted from the project for Global and regional Earth-system Monitoring using Satellite and in-situ data [GEMS: Schultz and Stein, 2006]**, **a soil moisture dependent** deposition parametrisation [Sanderson *et al.*, 2003], and a stratospheric ~~boundary condition~~**parametrisation** for H_2 and HD [Rahn *et al.*, 2003; McCarthy *et al.*, 2004; Pieterse *et al.*, 2011]. Our previous study [Pieterse *et al.*, 2011] was primarily focussed on the introduction and ~~general~~**global** evaluation of the new H_2 isotope chemistry scheme. Therefore, the global and latitudinal variability in H_2 were investigated using a single global model domain with a resolution of 6 by 4 degrees in the longitudinal and latitudinal directions, respectively. **In this study, the model performance is also evaluated for a model sub-domain with a resolution of 1 by 1 degrees over Europe.**

2.1. Surface emissions of H_2

In GEMS, the emissions related to fossil fuel use are separated into five categories: power generation, industrial combustion, road transport, an aggregated emission category that includes residential, commercial and other combustion processes [Schaap et al., 2005; Schultz et al., 2007], and emissions related to shipping [Endresen et al., 2003]. The GEMS emissions due

---

[4]School of Chemistry, University of

to biomass burning originate from a variety of sources such as wild fires, deforestation fires, bio fuel burning, agricultural waste burning, peat burning, and charcoal production/burning [Andreae and Merlet, 2001; Christian et al., 2003; van der Werf et al., 2003; Werf et al., 2010]. The spatial and temporal variability of the GEMS H_2 emissions from the ocean due to N_2 fixation are adopted from the spatial and temporal distributions of CO from the oceans [Erickson and Taylor, 1992]. The CO emissions are believed to be a robust indicator for the presence of biological activity, and therefore also for the presence of N_2 fixing microbial species such as Cyanobacteria. Similarly, the geographical distribution of biogenic CO emissions given by [Müller, 1992] is used to describe the spatial variability of emissions due to N_2 fixation on the continents by Rhizobia. Like in Pieterse *et al.* [2011], the different source fluxes are scaled to the average of previously reported global budget estimates [Novelli *et al.*, 1999; Hauglustaine and Ehhalt, 2002; Sanderson *et al.*, 2003; Rhee *et al.*, 2006; Price *et al.*, 2007; Xiao *et al.*, 2007; Ehhalt and Rohrer, 2009; Yashiro *et al.*, 2011]. With the resulting model framework, the global tropospheric cycle of H_2 and $\delta D\,[H_2]$ can be investigated along with 29 other chemical tracers implemented in the Carbon Bond Mechanism, version 4 [CBM-4, Gery *et al.*, 1988, 1989; Houweling *et al.*, 1998]. This feature can be used for imposing multi-species constraints upon the global budget of H_2. ~~In Pieterse et al. (2011), the global H_2 cycle was investigated by comparing the modelled H_2 mixing ratios and isotopic compositions with available measurements.~~ **In the following analysis, H_2 mixing ratios, isotopic compositions, and the known**

Bristol, UK

photochemical source magnitude of CO ~~mixing ratios~~ **are used to constrain the H_2 budget.**

2.2. Measurement data used for this study

Model values for the H_2 mixing ratios are compared with available data from a~~A~~ subset of stations from the EuroHydros project [Engel and EUROHYDROS PIs, 2009] **within the high resolution zoom region over Europe**, namely Mace Head [Ireland: Grant *et al.*, 2010], London [United Kingdom: Fowler *et al.*, 2011], Weybourne [United Kingdom], Cabauw [The Netherlands: Popa *et al.*, 2011], Gif sur Yvette [France: Yver *et al.*, 2009, 2011], Taunus [Germany], Heidelberg [Germany: Hammer and Levin, 2009], Jungfraujoch [Switzerland: Bond *et al.*, 2011], and Bialystok [Poland], see Figure 6. **The global scale performance for the H_2 mixing ratios is evaluated using flask sampling data from the CSIRO network measured at Alert (Canada), Cape Ferguson (Australia), Cape Grim (Australia), Casey Station (Antarctica), Macquarie Island (Australia), Mauna Loa (United States), Mawson (Antarctica), and the South Pole. For the global scale comparisons, the model results and continuous measurements are sampled between 11AM and 1PM local time. This way, the inherent discrepancies between the modelled values and the measurements due to sub grid level variability (the representation errors) and local influences are suppressed. Generally, the strongest vertical mixing occurs during this time of the day and measurements are thus less influenced by local soil uptakes or local sources. The noontime values**

---

[5]Centre for Australian Weather and

are therefore more representative for the large spatial and temporal scales. The latitudinal gradients in $\delta D\,[H_2]$ are investigated using existing data from ship cruises [Gerst and Quay, 2000; Rice *et al.*, 2010] and novel data from the EuroHydros project measured at Alert, Mace Head, Cape Verde, Amsterdam Island (France) and the South Pole [Batenburg *et al.*, 2011].

2.3. Meteorological data used for this study

In Pieterse *et al.* [2011], operational data from the European Centre for Medium-Range Weather Forecasts (ECMWF) were used for the simulations ~~in our previous study~~. In this work, **ECMWF ReAnalysis - Interim (ERA-Interim)** data are employed. These data show less ~~resolved and more realistic~~ vertical motion ~~exchange~~ which leads to much steeper surface gradients in the modelled H_2 mixing ratios. As will be shown in the result sections, this leads to a significant reduction in the modelled tropospheric burden of H_2. **It is not straightforward to determine which meteorological data are closest to reality for the time period between 2007 and 2008. The overview in Dee *et al.* [2011] shows that the operational and ERA-Interim model versions were the same at the start of the year 2007. Nevertheless, several updates were implemented in the operational model between 2007 and 2008. This leads to inconsistencies in the operational data for long term simulation periods and therefore, we prefer to use the ERA-Interim data in this work. Interestingly, the H_2 budget appears very sensitive to large scale vertical transport and an update of our previous implementation is required.** ~~It appears therefore necessary~~

Climate Research, CSIRO Marine and

~~to update our previous model implementation of the H_2 budget, including the isotopic composition [Pieterse et al., 2011]. In the following sections, we describe two substantial changes required in response to the recent studies published by Jordan and Steinberg [2011] and Batenburg et al. [2012], are described in the following sections.~~

2.4. Update of the new WMO calibration scale for H_2 mixing ratios

~~In the study by~~ Jordan and Steinberg [2011] **proposed** a new Global Atmospheric Watch (GAW) H_2 mole fraction calibration standard ~~was proposed~~. ~~The~~**This** MPI-2009 scale has recently been adopted by the WMO. Converting the original values for the H_2 mixing ratios measured by CSIRO to the MPI-2009 scale will increase the values by 3.5% [Jordan and Steinberg, 2011]. The data from the EuroHydros project are already calibrated against the MPI-2009 scale. As a result of this change, it is expected that the original H_2 scheme, introduced in our previous study [Pieterse *et al.*, 2011] and verified by NOAA/ESRL and CSIRO data, will underestimate the re-calibrated measured H_2 mixing ratios. ~~In our previous study, the measurements from NOAA/ESRL and CSIRO were not converted to a common scale because the reported difference between the two original calibration scales was considered negligible, *i.e.* 1.45% (Xiao, et al., 2007), in view of the precision of the measurements.~~

2.5. Update of the stratospheric boundary condition

Because the TM5 model ~~was~~**is** primarily designed for tropospheric studies, the stratospheric isotope chemistry scheme is incomplete. For instance, reactions of chemical species with electronically excited oxygen (O^1D), chlorine (Cl) and bromine (Br) radicals are not

Atmospheric Research, Australia

implemented. Especially the reactions with Cl and Br introduce stronger isotope effects in the CH_4 oxidation chain [Feilberg *et al.*, 2004; Mar *et al.*, 2007]. Therefore, a stratospheric boundary condition based on the parametrisation introduced by McCarthy *et al.* [2004] was used in Pieterse *et al.* [2011]. With this boundary condition, the modelled isotopic composition up to 100 mbar of +99‰ was corrected **(forced)** to a value of +128‰. This correction of the isotopic signature is rather large in view of the small impact of the stratosphere on the tropospheric burden of H_2 and stresses the importance of using sufficiently representative empirical relations to define the boundary condition. Here, upper tropo**s**heric/lower stratospheric measurements of $\delta D\,[H_2]$ from the CARIBIC program [Brenninkmeijer *et al.*, 2007] recently published by Batenburg *et al.* [2012] are used to update the original relation between the CH_4 mixing ratio (units in ppb) and the isotopic composition of H_2 (units in ‰ versus VSMOW) in the stratosphere to:

$$\delta D\,[H_2] = -0.350\,[CH_4] + 768. \tag{1}$$

Because it is actually HD that is traced by the model, this relation is first transformed into a relation between HD and CH_4. The stratospheric H_2 mixing ratio was set to 545 ppb following the adjustment to the MPI-2009 calibration scale. This results in the following relation for HD (units in ppb):

$$[HD] = -7.585 \times 10^{-5}\,[CH_4] + 0.338. \tag{2}$$

The required values for the CH_4 mixing ratios are obtained from the four-dimensional variational (4D-Var) data assimilation system implemented in

---

[6]School of Earth and Atmospheric

TM5 [Meirink *et al.*, 2008a, b]. These CH_4 fields also drive the isotope chemistry scheme. Using the values that are calculated with these parametric expressions, the **stratospheric** H_2 mixing ratio is then ~~calculated using~~**obtained from** the following expression (units in ppb):

$$[H_2] = \frac{1}{2\left(\delta D\left[H_2\right]+1\right)R_{VSMOW}}\left[HD\right]. \tag{3}$$

The factor 2 accounts for the fact that the isotopic composition is measured at a per atom basis. **Like in Pieterse *et al.* [2011], the following latitude (θ) dependent threshold pressure level p_s (Pa) separates the troposphere and the stratosphere:**

$$p_s = 3.00 \times 10^4 - 2.15 \times 10^4 \cos(\theta). \tag{4}$$

For all pressures below the threshold pressure level, the mixing ratios for H_2 and HD calculated by the default chemistry scheme are replaced by the empirical expressions that are described above. The model keeps track of the mass of H_2 and HD removed or added from or to the values obtained using the chemistry scheme. In this way, the stratospheric correction imposed by the stratospheric parametrisation can be calculated for the model domain up to 100 mbar used for the global budget calculations presented in Table 3. The flux of H_2 and HD across the 100 mbar model boundary is referred to as the vertical flux.

2.6. Update of the deposition parametrisation

By analysing the H_2 budget it was found that significant amounts of H_2 deposited on snow, oceans and wetted vegetation surfaces. In the default

Sciences, Georgia Institute of Technology,

implementation in TM5 [van Pul and Jacobs, 1994; Ganzeveld and Lelieveld, 1995; Ganzeveld et al., 1998] the large resistance values ($1{\cdot}10^5$ ms^{-1} sm^{-1}) for deposition to these surfaces were still small enough to allow for significant amounts of H_2 deposition, with deposition velocities up to 0.01 mms^{-1}. As a result, H_2 was also removed at these surfaces, whereas in reality, this does not occur because biological processes are suppressed in frozen environments and H_2 hardly dissolves in water.

We will discuss the impact of suppressing deposition of H_2 to these surfaces on the global budget. As the results will show, the dry deposition to vegetated tropical forests becomes extremely small when increasing the value for large resistances to $1{\cdot}10^9$ ms^{-1} sm^{-1}. This, in turn, is caused by the use of an in-canopy resistance deduced for ozone over maize crop by van Pul and Jacobs [1994]. They derived the following empirical formula for R_i:

$$R_i = 14\frac{LAI\, h_{can}}{u^*}. \tag{5}$$

In this expression, h_{can} (m) is the canopy height, LAI the leaf area index, u^* (ms^{-1}) the friction velocity, and 14 (m^{-1}) is an empirical factor. The expression is commonly used by many CTMs to calculate the impact of the vegetation canopies on the dry deposition of a given chemical species to the soils underneath. When applied for H_2, this parametrisation leads to very low deposition over tropical rainforests and Savannah regions, whereas in previous experimental studies [Conrad and Seiler, 1985; Yonemura *et al.*, 2000],

Atlanta, USA

large deposition velocities were observed for these regions. Since H_2 does not deposit to plants, a high canopy aerodynamic resistance over rainforests ($O\,[10^4]$ sm^{-1} with $LAI = 6$, $h_{can} = 30$ m, $u^* = 0.1$ ms^{-1}) is therefore not realistic, since intermittent transport processes refresh the air in the canopy roughly every one to two hours [Ganzeveld et al., 2002; Foken *et al.*, 2012]. We will therefore investigate the impact of reducing the empirical factor to 0.1m^{-1}. In this case, the R_i still scales with LAI, h_{can}, and $1/u^*$ but for typical rainforest characteristics, this will lead to a more realistic time scale of $R_i\,h_{can}$=5400 s or 1.5 hours for refreshing the air under the canopy.

2.7. Definition of scenario studies to reestablish a closed H_2 budget

The results from seven different scenario simulations of the TM5 model are analysed using data from the EuroHydros project. An overview of these scenarios is shown in Table 1. We run these scenarios to examine the effect of changing individual source and sink terms in the global budget on the temporal and latitudinal distribution of H_2 and HD in the troposphere, and compare the scenarios to available measurements. In order to close the H_2 budget, we will aim at a 14 Tg H_2/yr change in each of the most relevant sources and sinks. Subsequently, the model performance will be cross-validated for all scenarios using independent flask sampling data from CSIRO.

---

[7]Department of Air Quality and Climate

~~Several uncertainties in the H_2 budget can be exploited to re-close the budget and to obtain a good correspondence between the model and the observations over Europe. The most likely candidates to re-establish the H_2 budget in the new model formulation are (i) a reduction in the H_2 deposition (ii) an increase in the emissions as a result of fossil fuel burning.~~ The ~~first~~**reference** scenario, hereafter referred to as **S1**, ~~is used to determine the discrepancy between the modelled values obtained with~~**uses** the original (unchanged) H_2 isotope scheme [Pieterse *et al.*, 2011]~~ and the measured H_2 mixing ratios for a selection of stations from the EuroHydros project~~. Herein, **only** the impact of using the **ERA-Interim** data is included. In the second scenario **(S2)**, ~~the dry deposition velocities of H_2 are reduced to close the gap between the modelled values and observations, resulting in a reduction of 5 Tg H_2/yr, or 9%, in the deposition flux compared to the reference scenario (see Table 3)~~**the shut-down of the small remaining deposition to snow and water surfaces, wetted surfaces, vegetation leaf surfaces, and leaf mesophyll tissue is evaluated. Note that in scenario S2, the total deposition velocities are no longer scaled to 90%, as was the case for the results in Pieterse *et al.* [2011] and for scenario S1.** For the third scenario **(S3a)**, the ~~H_2 emissions due to fossil fuel burning are increased by an amount equal to the decrease in the second scenario. This corresponds to an increase of 29% in the emissions related to fossil fuel usage compared to the reference scenario (see Table 3)~~**in-canopy resistance for H_2 is decreased (see Section 2.6). Since this scenario leads to a small overestimate for the Antarctic stations, scenario S3b explores a reduction of the H_2 source from N_2 fixation (important over the SH oceans). Therefore, an additional global reduction**

Research at the Energy Research Centre of

of 2 Tg H_2/yr in these emissions is investigated by scenario S3b. In scenario S3c, the impact of increasing the deposition velocities for forest and Savannah ecosystem types by 10% on the SH H_2 mixing ratios and isotopic compositions is investigated. Because the NH H_2 mixing ratios and isotopic compositions were already on par with the measurements, the velocities to agricultural regions are decreased by 10% in scenario S3c to compensate for the increase in the deposition to forest regions.

~~Because there are no significant emissions due to biomass burning in Europe, it is not likely that an increase within the reported range of uncertainty will close the foreseeable gap between the model results and the re-calibrated H_2 mixing ratios.~~**Because the required adjustment for the tropospheric burden of H_2 is large compared to the magnitudes and ranges of uncertainty for the majority of the remaining sources and sinks in the H_2 budget, only two additional scenarios are explored to close the gap between the model results and the measurements. In scenario S4, the emissions of H_2 due to fossil fuel usage are reduced. It is noted that the required adjustment is very large, but on the other hand, the reported range for the H_2 emissions due to fossil fuel burning (5–25 Tg H_2/yr) is also large, see Table 3. Therefore, it still makes sense to at least investigate the impact of such a change on the model performance. With scenario S5 we will try to close the budget by increasing the H_2 sink from OH oxidation. An increase of 53% in the rate constant is needed to achieve the required reduction of 9.5 Tg H_2/yr in this sink term. This scenario, however, is considered unlikely,**

the Netherlands (ECN), Petten, The

because the rate constant for the~~The removal rate associated with the second sink process, namely the~~ photochemical removal of H_2 by ~~the hydroxyl radical (OH),~~**OH** is

Netherlands

[8]Laboratoire des Sciences du Climat et de l'Environnement (LSCE), Gif-sur-Yvette, France

[9]Max-Planck Institut für Biogeochemie, Jena, Germany

[10]Institut für Meteorologie und Geophysik, Goethe-Universität Frankfurt, Frankfurt, Germany

[11]Department of Earth Sciences, Royal Holloway, University of London, Egham, UK

[12]Empa, Swiss Federal Institute for Materials Science and Technology, Laboratory for Air Pollution/Environmental Technology, Duebendorf, Switzerland

[13]Institut für Umweltphysik, Heidelberg Universität, Heidelberg, Germany

[14]School of Environmental Sciences, University of East Anglia, Norwich, UK

well known [Sander *et al.*, 2006]. Furthermore, ~~as shown recently by Pieterse et al. [2011], the atmospheric lifetime of CH_4 (8.3 years)~~**the chemical lifetime of 8.6 years for the reaction of CH_4 with OH** is adequately reproduced by the TM5 model. This indicates that the modelled mixing ratios of OH are realistic as well.~~Hence, it is unlikely that the photochemical removal of H_2 is too strong.~~

~~Increasing~~**Decreasing** the photochemical production of H_2 is not considered because the source magnitude is in line with expectation for **scenario S1. A reduction of the photochemical source magnitude by the required amount to close the H_2 budget will lead to an overall photochemical source strength for H_2 that is incompatible with the atmospheric budget of CO [Ehhalt and Rohrer, 2009].** ~~the reference scenario. Increasing the photolysis reaction rate might lead to an overall photochemical source strength for H_2 that cannot be supported by the findings of the above mentioned studies. Finally, the magnitudes and ranges of uncertainties of the H_2 emissions due to N_2 fixation in the soils and oceans are too small to be relevant in view of the anticipated changes to reestablish a closed H_2 budget.~~**Other separate scenarios, *i.e.* reducing the H_2 emissions due to N_2 fixation, would require changes that are outside the established error margins for these sources.**

2.8. Quantifying the agreement between the model results and observations

In all comparisons discussed in the next sections, the agreement between the model results and the measurements is quantitatively analysed by using the chi-squared value (χ^2) as a metric [Meirink *et al.*, 2008b; Villani *et al.*,

2010], calculated as:

$$\chi^2 \equiv \sum_{i=1}^{n} \frac{(x_i - y_i)^2}{\sigma_i^2}, \tag{6}$$

where $i \in [1, n]$ is the index of measurement i with a value of y_i approximated by the model value x_i for a set of n measurements. The square of the variance σ_i is calculated by:

$$\sigma_i^2 \equiv \sigma_{x,i}^2 + \sigma_{y,i}^2. \tag{7}$$

The uncertainty in the observations $\sigma_{y,i}$ is calculated using the following expression:

$$\sigma_{y,i}^2 \equiv \sigma_{meas,i}^2 + \sigma_{y,time,i}^2. \tag{8}$$

The measurement uncertainty $\sigma_{meas,i}$ is estimated at 2% for the measured H_2 mixing ratios and at 5‰ for the measured isotopic compositions. In the case that time averaging is used to calculate a measured value y_i, the standard deviation $\sigma_{y,time,i}$ over the time averaging period is calculated. The uncertainty in the model results $\sigma_{x,i}$ is calculated by:

$$\sigma_{x,i}^2 \equiv \sigma_{trans,i}^2 + \sigma_{sub,i}^2 + \sigma_{x,time,i}^2. \tag{9}$$

Here, the uncertainty due to errors in atmospheric transport $\sigma_{trans,i}$ is estimated by calculating the standard deviation over a model value x_i obtained by three different interpolation methods [Bergamaschi *et al.*, 2005]. The uncertainty due to sub-grid variability in processes like emissions and planetary boundary layer (PBL) height ($\sigma_{sub,i}$) is estimated at 2% for the H_2 mixing ratios calculated for background stations, and at 5% for continental stations.

For $\delta D\,[H_2]$, we adopt $\sigma_{sub,i}$=11‰ because only a small fraction (≈10%) of the uncertainties in the H_2 and HD mixing ratios is not correlated. For example, H_2 and HD and are both emitted as a result of biomass burning. Because the isotope signature is a fixed value, a fixed ratio exists between the emitted amounts of H_2 and HD. Therefore, only the uncertainty in the isotope signature propagates into the uncertainty in the modelled isotopic composition. In the case that time averaging is used to calculate a modelled value x_i, the standard deviation $\sigma_{x,time,i}$ of the model values is calculated over the time averaging period.

Because the number of observations determine the overall value of χ^2, it is useful to scale it by the number of degrees of freedom ($\nu = n - 1$) which yields the reduced chi-squared value:

$$\tilde{\chi}^2 \equiv \frac{\chi^2}{\nu}. \tag{10}$$

This way, the goodness of fit of model results to different data sets can be compared using a normalised statistical value. Generally, a value of $\tilde{\chi}^2$ that is much larger than unity indicates a poor agreement between the model results and the measurement data.

3. Results

In the following sections, the model results produced by the ~~reference scenario, reduced deposition scenario, and increased fossil fuel burning emission scenario (increased fossil fuel emission scenario)~~**seven scenarios (see Table 1) are evaluated using available measurements**. The analysis starts by comparing the modelled and measured seasonal

variability in the H_2 mixing ratios for ~~a selection of stations from~~ the EuroHydros and CSIRO ~~networks~~**stations**. Section 3.2 evaluates the modelled latitudinal variability in $\delta D\,[H_2]$ using available measurements. **Subsequently, the regional short-term variability in the EuroHydros H_2 measurements is investigated in Section 3.3. The overall implications of this analysis for the global budget of H_2 and are presented in Section 4**.

3.1. Seasonal variability in H_2

In Figure 1, the TM5 model results are compared to the measurements from the EuroHydros project. **Table 2 lists the quantitative measure ($\tilde{\chi}^2$) for the agreement between the model results and the measurements.** ~~It is clear that the~~**The** reference scenario **(S1, black dotted line)** consistently underestimates the measured H_2 mixing ratios.

~~A global reduction in the calculated dry deposition velocities (S2) from 90% to 75% of the values calculated using the original implementation of the scheme [Sanderson et al., 2003], leads to the best possible overall agreement between the model results and observations (blue lines). This leads to an overall reduction of 5 Tg H_2/yr, or 9%, in the deposition flux compared to the reference scenario. The reason why this relative change in the deposition flux is smaller than in the change in the deposition velocities is caused by the inhomogeneous distribution of the calculated H_2 mixing ratios in the~~ **PBL** ~~over regions influenced by deposition. The reduction in the deposition velocities is rather large but the uncertainty of the underlying measurements [Conrad and Seiler, 1985; Yonemura et al., 2000] for the original deposition parametrisation is also significant (>30%). Using an effective Earth soil surface area for deposition of 90×10^6 km^2 [Novelli et al., 1999], the~~

~~derived global average deposition velocity yields 4.0×10^{-2} cm s^{-1}. This value is well in the range of previously reported deposition velocities, extensively summarised by Ehhalt et al. [2009].~~

In contrast, increasing the deposition resistance values for snow and water surfaces, wetted surfaces, vegetation leaf surfaces and leaf mesophyll tissue (S2, black dashed line) leads to a large overestimation in the modelled H_2 mixing ratios. Thus, deposition is clearly underestimated in this scenario. Reducing the in-canopy deposition resistance (S3a, blue lines) leads to much better agreement with the observations, especially at the background stations (*e.g.* at Mace Head and Jungfraujoch). Remaining discrepancies between the model results and the non-background observations in Figure 1 (*e.g.* at Cabauw and London) can be attributed to the limited model resolution and are further explored in Section 3.3~~and more specifically for Mace Head in Section 3.5~~. **As expected, the lower in-canopy resistance combined with lower ocean H_2 emissions due to N_2 fixation (S3b, orange lines) leads to agreement between the model and the measurements similar to scenario S2b. This is also the case when the soil deposition velocities for forest and Savannah ecosystems are increased whereas the velocities are decreased for agricultural regions (S3cm red lines). Decreasing the fossil fuel emissions (S4, magenta lines) leads to a very poor model performance, especially for London and the other low-altitude continental stations. Increasing the photochemical removal of H_2 by OH (S5, purple lines) also appears an efficient method to improve the agreement between the model and measurements.**

These findings are confirmed by the $\tilde{\chi}^2$-values in the first row of Table 2. The value of 0.9 for $\tilde{\chi}^2$ confirms that scenario S3a is in good agreement with the observations and that for scenarios S3b and S3c, a similar performance is achieved. The large $\tilde{\chi}^2$-value of 2.9 obtained for scenario S4 confirms that reducing the fossil fuel emissions does not lead to a better model performance. Of course, this does not exclude the possibility that a combination of changes in the different processes will lead to a better agreement with the observations, as for example in scenario S3b, but it clearly suggests that a substantial part of the mismatch between scenario S2 and the observations is attributable to too little removal of H_2, either by deposition or by photochemistry.

~~The increased fossil fuel emission scenario leads to an improvement compared to the reference case but the gap is not closed completely (red lines in Figure 1). This is because an increased mixing ratio in the PBL also leads to an increase in deposition and photochemical removal, as will be further detailed in Section 4. The comparison of the scenario results with the independent data provided by CSIRO confirms that reducing deposition leads to the best overall agreement (blue lines in Figure 2). In particular in the Southern Hemisphere (SH), increased fossil fuel emission scenario is less efficient than the reduced deposition scenario. Further increasing the emissions related to the use of fossil fuels would probably fully close the gap between the model but as Section 4 will show, this is not a plausible scenario.~~

The comparison of the scenario results with the independent data provided by CSIRO shows that scenario S3a (blue lines) slightly overestimates the H_2 mixing ratios for the stations on or near Antarctica. This suggests that either

too much H_2 is emitted or too little H_2 is removed on the SH. In our previous study, the model results showed better correspondence with the measurements performed at the South Pole. This might have been caused by the erroneous uptake of H_2 due to deposition to the SH oceans. One budget term that can offset these high southern latitude H_2 levels are the H_2 emissions from the oceans. Indeed, reducing the H_2 emissions due to nitrogen fixation to the oceans (S3b) shows a slight improvement in the agreement between the model results and observations. This improvement indicates that the emission source strength of 5 Tg H_2/yr due to N_2 fixation in the oceans might be too large, possibly only for the Arctic and Antarctic regions, as suggested earlier by Herr *et al.* [1981, 1984]. Alternatively, the overestimation could be caused by the larger vegetation resistances in the corrected deposition scheme resulting in much lower deposition velocities calculated the rainforest and Savannah ecosystems than calculated in Pieterse *et al.* [2011]. Indeed, the agreement also improves by increasing the deposition velocities for the forest and Savannah ecosystem types (S3c). The results obtained with the scenario S4 and S5 are slightly worse than the results obtained with scenario S3a–S3c, which is reflected by the larger $\tilde{\chi}^2$-values (1.3 and 1.4, respectively) in the second row of Table 2. Overall, scenario S3b and S3c lead to the best agreement ($\tilde{\chi}^2$=1.0).

Just as in our previous study [Pieterse *et al.*, 2011], the model does not ~~precisely~~ capture the seasonal cycle at Alert **well** because it assumes that **little or** no deposition will occur in (partly) snow covered regions. Hence, deposition ~~will~~ starts affecting the modelled H_2 mixing ratios three months later in the season than observed in the measurements. The

measurements at Mauna Loa show more variability than captured by the model because of the very coarse model resolution (6 by 4 degrees) at that location. As the largest part of the surface of the corresponding grid cell lies above the Pacific Ocean, the model~~led values~~ cannot capture the effect of local emissions from Hawaii on the measured H_2 mixing ratios.

3.2. Latitudinal variability in $\delta D\,[H_2]$

Figure 3 shows the modelled latitudinal gradient in $\delta D\,[H_2]$, sampled at the oceanic meridians, compared to available measurement data. ~~The model results using the new stratospheric parametrisation yield a much better agreement with the measured isotopic compositions, especially when combined with the reduced deposition scenario S2 (blue line) and S6 (purple line). Increasing the emissions related to fossil fuel usage (red line) also improves the agreement between model and observations on the SH, but in the NH the model still underestimates the measured isotopic signature.~~

The results of scenario S2–S3c are in much better agreement with the observations than scenario S1. This is partly caused by the new stratospheric parametrisation. Depending on the CH_4 mixing ratio, the parametrised stratospheric values for $\delta D\,[H_2]$ are >10‰ larger in this work than the values obtained with the parametrisation used in Pieterse *et al.* [2011]. The actual corrections imposed by the new stratospheric parametrisation are discussed in Section 4. The $\tilde{\chi}^2$-values for the isotope results are shown in the third row of Table 2. Because the uncertainty in the measurement data is large, it is not possible to make a statistically sound distinction between scenarios S2–S3c. It how-

ever obvious that scenarios S4 and S5 do not agree with the measurements, especially for the NH.

~~Further~~**A more quantitative comparison between scenarios S2–S3c can be found in** ~~support for scenario S2 can be found in~~ the seasonal evolution of the modelled latitudinal gradient of $\delta D\,[H_2]$ and H_2 mixing ratios measured at 5 stations (Alert, Mace Head, Cape Verde, Amsterdam Island, and the South pole) in the EuroHydros project [Batenburg *et al.*, 2011], averaged for the years 2007 and 2008 (see Figure 4). **Again, it is clear that scenarios S4 and S5 do not lead to realistic values for $\delta D\,[H_2]$ and are therefore not further discussed here. The $\tilde{\chi}^2$-values for the goodness of fit of the isotopic compositions in the fourth row of Table 2 show that scenarios S2–S3c are in good agreement with the observed mean latitudinal gradient of $\delta D\,[H_2]$. At the same time, the $\tilde{\chi}^2$-values for the accompanying H_2 mixing ratios shown in the fifth row of Table 2 are poor for scenarios S2 and S3a. Thus, scenarios S2b and S2c show the best performance for the H_2 mixing ratios and isotopic compositions that were measured simultaneously at the EuroHydros stations.**

The seasonal mean values assigned to the highest NH latitude are obtained using measurements from Alert. Here, the discrepancy between the results of both model scenarios and the observed seasonal cycle is again attributed to the fact that in TM5, it is assumed that deposition in the snow-covered **regions** does not occur (see Section 3.1).

Another clear feature is the consistent negative bias relative to the observed isotopic composition at the highest SH latitudes (also visible in Figure 3)**, except for scenario S3b.**~~, although the H_2 mixing ratio is modelled well. At these high~~

~~SH latitudes, deposition and surface sources cannot directly influence the isotopic compositions.~~**However, it appears that reducing the global emission source strength for H_2 due to N_2 fixation processes in the oceans leads to too large values for $\delta D\,[H_2]$ at the mid latitude stations. Possibly, these emissions are only overestimated for the Arctic and Antarctic regions [Herr *et al.*, 1981, 1984]**. The larger values for the isotopic composition might ~~instead~~**also** be explained by the exchange of tropospheric air with stratospheric air that is much more enriched in HD in the Antarctic region than at the lower SH latitudes. The modelled isotopic composition from 30°S to 90°S is very sensitive to the isotopic composition that is assumed for the stratosphere from 60°S to 90°S [Pieterse *et al.*, 2011]. For this region, a negative bias of 10‰ between the modelled surface values and observations, as shown in Figure 4, can be explained by underestimating the isotopic composition in the stratosphere by 20‰. Possibly, this is related to the CH_4 background values that are used to calculate the stratospheric boundary condition. At latitudes above 60°S, these fields show CH_4 mixing ratios at the tropopause that are up to 25% lower than for instance a climatology obtained from the Halogen Occultation Experiment [Grooß and Russell III, 2005]. **This can be the result of model transport errors in the STE [Noije et al., 2004; Pieterse *et al.*, 2011]**. In view of Equation 1, these discrepancies could easily explain why the SH isotopic compositions are underestimated by the current TM5 model setup. As the differences between the modelled and observed H_2 mixing ratios are small, it is not expected that this discrepancy is of large importance for closing the global H_2 budget.

~~For the reduced deposition scenario, the overall correction is small in terms of contribution to the overall isotopic composition up to a pressure height of 100 mbar~~

~~(+2‰ instead of +59‰), see Table 3 in Section 4. At the same time, the increased fossil fuel emission scenario requires a correction of +52‰. Thus, the reduced deposition scenario driven by **ERA-Interim** data requires less stratospheric forcing to match the model results with the global observations at the surface as well as the lower stratosphere. In other words, this scenario explains a significant part of the observed variability in H_2 and $\delta D\,[H_2]$.~~

3.3. Regional scale variability in H_2 over Europe

~~In this section, the model results obtained using the high resolution model sub-domain over Europe are analysed for the years 2007 and year 2008.~~Figure 5 shows the aggregated hourly average H_2 mixing ratios as a function of ECMWF surface wind direction for ~~a selection of~~**the** 8 EuroHydros stations where continuous measurements were performed. The median, upper quartile, 95th percentile, lower quartile, and 5th percentile were calculated over all values attributed to each wind sector. The median is shown as the white horizontal line in each coloured bar that is bound by the lower and upper quartile. The 5th percentile and 95th percentile are shown as whisker lines. **Scenarios S1, S2, S3a and S4 and S5 are not shown in the figure because their overall performance for the EuroHydros stations was poorer than for scenario S3b and S3c (see Section 3.1). Because scenario S3b and S3c showed a similar performance, only the results of scenarios S3c are shown here for clarity.**

~~As before, the reference scenario (black) consistently underestimates the measured H_2 mixing ratios (green) whereas the reduced deposition scenario (blue) shows the best overall agreement with the observations.~~ The modelled values for this scenario show a good correspondence with the measurements, with the exception of specific wind directions,

e.g. the East to South-East wind sector for the station at Cabauw. ~~In these cases, both the reduced deposition scenario as well as the increased fossil fuel emission scenario (red) either significantly over- or underestimate the measured values and variability.~~ To further investigate the causes for these discrepancies, the differences between the modelled ~~median values of the reduced deposition scenario and the~~**and** observed median H_2 mixing ratios are shown as coloured wind roses in a map plot in Figure 6.

At Mace Head [Grant *et al.*, 2010], the modelled median H_2 mixing ratios corresponding to the marine sector (South to North-West) agree well with the measurement data, whereas the model underestimates the observations in the land sector. This indicates again that either deposition is overestimated or that the surface emissions are underestimated. The results for the station **in Egham** located West to South-West of London are clearly affected by the fact that the model grid cell containing this station also contains a highly populated urban area (and the associated emissions) whereas the station itself is located in a rural area West of the London city centre. As a result, the measurements affected by the emissions from London city (Easterly wind sector) are relatively well captured by the model, whereas the model results from the other wind directions overestimate the measured H_2 mixing ratios. ~~The results of the increased fossil fuel emission scenario are slightly better for the measurements affected by the emissions from London city. The other wind directions also improve because deposition is also stronger in this scenario.~~

The measurements performed at the tall tower station near Cabauw in The Netherlands are strongly influenced by urban activity [Popa *et al.*, 2011]. Contrary to the station near London, the station at Cabauw is located in a grid cell with much less urban influence than representative for this site. In reality, the measurements are severely influenced by

emissions originating from the urban and industrial areas in Utrecht (The Netherlands), the Ruhr area (Germany), and Antwerp (Belgium), from the Northern to South-Westerly wind directions, respectively. Hence, the model results in the marine sector (West to North) are in closest agreement with the observations, while the measurements are underestimated for other wind directions.

For similar reasons, the measurements at Gif sur Yvette are underestimated in the wind sector where the station is influenced by the city of Paris **(North to North-East)**. At Weybourne (United Kingdom), the signals arriving from the urban area of Norwich, South-East of the station, are adequately captured by the model. For the Southern to Western wind directions, the model overestimates the H_2 mixing ratios because the emissions in the grid-cell containing the Weybourne station are larger than representative for these wind directions. Similarly, deposition is overestimated for the Northern to Eastern wind directions.

In Heidelberg **and Taunus** (Germany), the model results are generally in good agreement with the **observations, as is the case for the observations at the Jungfraujoch in Switzerland [Bond *et al.*, 2011]**.~~measurement results, with the exception of the measurements influenced by air masses arriving from the area of Stuttgart located East to South-East of the station. The overestimated values for the modelled H_2 mixing ratios in Figure 5 suggest that the emissions that are implemented for this area are probably overestimated, while the emissions of other anthropogenic sources such as Heidelberg City, or the industrial regions in the North-West are well represented. At Taunus, also in Germany, the results for the reduced deposition scenario agree well with the measurements, as is the case for the measurements performed at the Jungfraujoch in~~

~~Switzerland [Bond et al., 2011].~~ For the station located North-West of Bialystok (Poland), the model underestimates the measured H_2 mixing ratios arriving from the city nearby the tower. **The H_2 mixing ratios in air**~~Air~~ masses arriving from the East and North-East ~~are very likely influenced by~~**are also underestimated, which means that the** deposition of H_2 to the large evergreen forest and arable regions in the direct vicinity East and North-East of the station **is overestimated.**

The $\tilde{\chi}^2$-values in the sixth row of Table 2 confirm that scenarios S3b and S3c show the best overall agreement with the continuous observations from the EuroHydros project. Scenario S5 is not considered here because of its poor performance for the comparisons in the previous sections. More detailed analysis on the main contributors to the overall $\tilde{\chi}^2$-values revealed that none of the model scenarios produces realistic values for the station at Egham. Indeed, removing the data from this station results in $\tilde{\chi}^2$-values closer to unity, see seventh row in Table 2. ~~In all, the model results for the reduced deposition scenario compare well with the available measurement data.~~ The remaining discrepancies between the model results and the measurement data can in general be attributed to the limited representativeness of the relatively coarsely gridded model surface emissions and deposition mass fluxes for capturing certain station specific local influences. Such representation errors were also found in integrated model studies investigating other species, for example carbon dioxide [Patra *et al.*, 2008].

4. Implications for the global budget

Table 3 shows the global budgets for the year 2008 of ~~the reference scenario, the reduced deposition scenario and the increased fossil fuel emission~~**all seven** scenario**s**, along with

a selection of previously derived budgets. The atmospheric burden **of 165 Tg H_2** associated with the ~~reduced deposition scenario (S2, 165 Tg H_2)~~ **scenarios that agree best with the observations, *i.e.* scenario S3b and S3c,** is significantly larger than the burden for the reference scenario (S1, 154 Tg H_2). This increase of 7.1% is ~~much~~ larger than corrections related to the calibration scale revision (see Section 2.4) and requires further explanation.~~The budget of the two-way nested setup of the TM5 model with a high resolution zoom over Europe and the Northern part of Africa used for this study yields a slightly different global budget compared to the previous setup.~~ Due to slower vertical mixing associated with the use of **ERA-Interim** data,~~much~~ steeper near-surface gradients are obtained **because the calculated PBL heights are on average 10% smaller**. This leads to near-surface mixing ratios that are ~~much~~larger compared to the free tropospheric mixing ratios ~~. This results~~ **and, as a consequence, to**~~in~~ stronger removal of H_2 by deposition compared to the previous model setup (see Table 3)**.** ~~and~~ ~~t~~**Therefore,** the **modelled** tropospheric burden is smaller for scenario S1.

~~We conclude from this analysis that the deposition velocities used in our previous study, despite being scaled down to 90% of the original values from Sanderson et al. [2003] already, appear to be too large. Decreasing the deposition velocities further to 75% of the original values leads to an increase of 11 Tg H_2 in the tropospheric burden. The new stratospheric parametrisation (see Section 2.5) for the H_2 mixing ratio adds another 2 Tg H_2, leading to an overall increase of 11 Tg H_2 in the tropospheric burden.~~

The difference between the results of scenarios S1 and S2 shows the impact of using larger resistance values ($1{\cdot}10^5$ ms^{-1} sm^{-1}) for the deposition of H_2 to snow and water surfaces, wetted surfaces, vegetation leaf surfaces, and leaf

mesophyll tissue. Clearly, the values for the tropospheric burden and atmospheric lifetime (176 Tg H_2 and 2.6 years) obtained with scenario S2 are too large. At the same time, the correction required for the stratospheric isotopic compositions of -137‰ also shows that values obtained for $\delta D\,[H_2]$ in the stratosphere are unrealistic. Reducing the in-canopy resistance term (scenario S3a) drastically improves the overall model performance. The results in the previous sections showed that the remaining gap of 2 Tg H_2 between scenario S3a and scenario S3b or S3c is likely caused by either too little removal or too large emissions on the SH; reducing the H_2 emissions due to N_2 fixation in the oceans (scenario S3b) further improves the model performance. The approach of decreasing the soil deposition resistances for forest and Savannah ecosystem types (scenario S3c) leads to a comparable improvement. Alternatively, decreasing the biomass burning emissions could improve the agreement between the model and the observations of H_2. This would probably also increase the isotopic compositions on the SH, leading to a better agreement with the observations of $\delta D\,[H_2]$, as was the case for scenario S3b.

Overall, the updated stratospheric ~~boundary condition~~**parametrisation** imposes a smaller correction on the results produced by the stratospheric H_2 chemistry scheme **in scenario S3a–S3c** than the previous version implemented in the reference scenario (~~less than~~**around** 1.0 instead of 2.4 Tg H_2). Also, the results **produced by scenario S3c** ~~using the new stratospheric boundary condition~~ require ~~only a small~~ **no** correction in the isotopic composition **from the stratospheric parametrisation**~~ of 2‰. Thus, the slower vertical transport in the driving~~ **ERA-Interim** ~~meteorology results in a more~~

~~consistent H_2 budget predicted by the TM5 model.~~ **That is, scenario (S3c) driven by ERA-Interim data explains an important part of the observed variability in H_2 and $\delta D\,[H_2]$.**

~~An increase of 9 Tg H_2 in the fossil fuel usage related emissions would be required to match the tropospheric burden calculated by the reduced deposition scenario.~~ **The analysis in Section 3.1 and Section 3.2 showed that the agreement between the modelled H_2 mixing ratios and isotopic compositions and the observations from the EuroHydros network was very poor for scenario S4. Moreover, the**~~The~~ resulting ~~overall~~ fossil fuel emission source magnitude of ~~26.0 Tg H_2/yr~~**3.2 Tg H_2/yr** is outside the **reported** range of ~~7~~**5**–25 Tg H_2/yr~~reported by a large number of studies~~ (see Table 3), and is therefore considered **unrealistic.**~~less probable. Moreover, the resulting isotopic composition up to 100 mbar without the correction due to the stratospheric parametrisation is estimated at +96‰. This value is much smaller than the value of +140-2=+138‰ produced by the reduced deposition scenario.~~

For similar reasons, it is also not obvious to close the global budget by increasing the photochemical removal (scenario S5). In order to obtain the required increase of 9.5 Tg H_2/yr in the photochemical removal of H_2, the rate coefficients of the reactions of H_2 and HD with OH had to be increased by 53%. This perturbation is outside the range of uncertainty of ±10% reported by Sander *et al.* [2006]. Furthermore, the resulting overall sink of 34.1 Tg H_2/yr is outside the range of 14–24 Tg H_2/yr reported in earlier studies, see Table 3.

A scenario to investigate the impact of reducing the photochemical source to 23 Tg H_2/yr was not considered because this approach would imply an unreal-

istically low photochemical source for CO from formaldehyde. Like H_2, CO is photochemically produced from formaldehyde and therefore, the photochemical source magnitudes of both species are intertwined [Sander *et al.*, 2006]. Contrary to H_2, the photochemical source magnitude of CO is well constrained because deposition plays only a minor role in the removal of CO from the atmosphere [Houghton *et al.*, 2001]. In this TM5 model setup, 1.24 Pg CO/yr is produced from formaldehyde, which is in good agreement with the photochemical source magnitudes of 1.24 and 1.29 Pg CO/yr reported by Houghton *et al.* [2001] and Kopacz *et al.* [2010], respectively. In all, the TM5 chemistry scheme produces 34 Tg CO per Tg H_2 from formaldehyde, which also agrees well with the expected ratio of 36 Tg CO per Tg H_2 reported by Ehhalt and Rohrer [2009]. A reduction of the photochemical source strength for H_2 to the above mentioned value would therefore yield a photo chemical source strength for CO between 0.78 and 0.83 Pg CO/yr. These values would be too small in view of the reported values.

For similar reasons, Ehhalt and Rohrer [2009] have postulated that the budgets reported by Rhee *et al.* [2006] and Xiao *et al.* [2007], see Table 3, might be compromised by an unrealistically large photochemical source of H_2 compared to what is expected from the photochemical source of CO. ~~The modelled background CO mixing ratios presented in Section 3.5 are too low because the CO emissions used in this model version of TM5 are too small (Huijnen et al., 2010). The CO emissions due to fossil fuel, bio fuel, and biomass burning add up to 706 Tg CO/yr instead of the established value of 1350 Tg CO/yr (Houghton et al., 2001; Kopacz et al., 2010). It is also lower than the~~

~~value of 1110 Tg CO/yr recently estimated using the 4D-Var data assimilation system implemented in TM5 (Hooghiemstra et al., 2012). However, only the photochemical source magnitude of CO is relevant to validate whether the photochemical production of H_2 is realistically modelled by TM5.~~Using the ratio of 34 Tg CO per Tg H_2, the photochemical source magnitudes for H_2 of Rhee *et al.* [2006] and Xiao *et al.* [2007] in Table 3 imply photochemical source magnitudes of 2.17 and 2.61 Pg CO/yr, respectively. These magnitudes are a factor of 1.7 and 2.1 larger than the present-day estimates and indicate that a photochemical source magnitude of 37 Tg H_2/yr would have been more realistic. **Because this analysis is performed by using a chemical reaction mechanism implemented in a full global CTM, these results form an independent confirmation of the conclusion by Ehhalt and Rohrer [2009] that the above mentioned large estimates for the removal of H_2 by deposition should not be used for future studies.**

~~Therefore, also from the perspective of the isotopic compositions,~~**Since** ~~the reduced deposition~~ scenario **S3c produces the most realistic values for the H_2 mixing ratios, requires** ~~less~~**little stratospheric forcing for the H_2 mixing ratios and isotopic compositions, deposition is identified as the most sensitive parameter to re-establish a closed**~~the~~ **global H_2 budget. Because of the high impact of deposition on the budget, the vertical transport in the model plays a very important role for H_2 in the troposphere. The magnitude of the deposition term in the budget shows a strong dependency on the vertical transport, indicating that H_2 and its isotopic signature put important constraints on atmospheric transport processes such as STE.**~~stratosphere-troposphere exchange.~~

5. Conclusions

We have further tested and updated the molecular hydrogen (H_2) isotope chemistry scheme in the two-way nested TM5 model [Krol *et al.*, 2005; Pieterse *et al.*, 2011].~~using measurements from the European EuroHydros project and measurements of the isotopic composition in the stratosphere performed within the CARIBIC program. Additional CSIRO data were used to independently evaluate the model performance. All H_2 measurements used in this study are calibrated to the MPI-2009 calibration scale recently adopted from Jordan and Steinberg [2011]. At the start of this study,~~**In a first simulation (scenario S1)** with the reference H_2 chemistry scheme ~~underestimated~~ the atmospheric burden of H_2 **was underestimated** by 7.1%. This percentage is larger than the differences of 2.0–3.5% between the MPI-2009 scale and the old calibration scales. The additional gap is a consequence of using **ERA-Interim** meteorology for the model simulations described in this study. These data ~~show less resolved vertical exchange than the operational data used in our previous study, and produce larger~~ **show more atmospheric stability resulting in increased values for the** near-surface H_2 mixing ratios compared to the free tropospheric mixing ratios. As a result, the removal of H_2 by deposition increases ~~, leading to the observed decrease in~~ **and** the modelled atmospheric burden of H_2 **decreases**.

During this research, we found that our previous study [Pieterse *et al.*, 2011] overestimates the H2 deposition to snow, water and vegetation surfaces. Avoiding deposition to these surfaces leads to an overestimate of the tropospheric burden of 6.7% (S2). We propose a reduced in-canopy resistance, corresponding with canopy mixing times of 1–2 hours, to describe the trans-

port of H_2 through the canopy to the soil underneath. We further explored scenarios in which the H_2 emission from N_2 fixation is reduced. Indeed, we are able to close the H_2 budget and to obtain a good correspondence with available H_2 and $\delta D\,[H_2]$ observations. Deposition is identified as the process to which the H_2 budget is most sensitive. Other processes, such as fossil fuel emissions and oxidation by OH require much larger perturbations to close the H_2 budget. Thus, uncertainties in these parameters may play a role, but the required perturbations for single processes are often outside their established uncertainty ranges.

~~Two scenarios were considered to re-close the H_2 budget. In the first scenario, the removal by deposition was reduced by 5 Tg H_2/yr whereas in the second scenario, the emissions related to the usage of fossil fuels were increased by an equal amount. Comparison of the modelled H_2 mixing ratios with the monthly median values of the data from the EuroHydros and CSIRO networks show a much better performance for the reduced deposition scenario than for the increased fossil fuel emission scenario, see Section 3. Additionally, the modelled values of $\delta D\,[H_2]$ in the increased fossil fuel emission scenario require a much larger stratospheric correction to match the model results to the measured stratospheric isotopic compositions. The reduced deposition scenario requires only a small correction of +2‰. The performance of the reduced deposition scenario is also very satisfactory for the regional scale. Discrepancies between the model results and the measurements are mainly related to the limited representativeness of the model for capturing certain station specific local influences due to limited resolution.~~

~~Because the reduced deposition~~**All in all,** scenario **S3c** produces the most realistic model results for H_2 and $\delta D\,[H_2]$, it is adopted to update the global budget of H_2 previously reported in Pieterse *et al.* [2011]. The tropospheric burden is now estimated at 165 Tg H_2, and the magnitudes of removal of H_2 by deposition and photochemical oxidation at 53 and 23 Tg H_2/yr, respectively. This results in a tropospheric lifetime of 2.2 yr. The photochemical production is estimated at 37 Tg H_2/yr. ~~Perturbing the magnitudes of the above mentioned sources and sinks by more than a few Tg H_2/yr, leads to significant differences between the modelled values and observations of H_2 mixing ratios and isotopic compositions.~~**The obtained agreement between the modelled and measured H_2 mixing ratios and isotopic compositions is very sensitive to relatively small perturbations ($\leq$5 Tg H_2/yr) in the removal of H_2 by dry deposition.** It is therefore expected that the proposed budget provides a sufficiently accurate baseline scenario to evaluate the impact of increasing H_2 emissions on tropospheric chemistry and climate.

Acknowledgments. This project was supported by the EuroHydros project, funded via the Sixth Framework Programme of the European Commission (SUSTDEV-2005-3.I.2.1 Atmospheric composition change: Methane, Nitrous Oxide and Hydrogen). Further support was provided by the Pan-European Gas-AeroSOl-climate interaction Study (PEGASOS), funded by the European Commission under the Seventh Framework Programme (FP7-ENV-2010-265148). Andrew Rice from Portland State University (USA) and Paul Quay from the University of Washington (USA) are acknowledged for access to their H_2 isotope data. Finally, the Nederlandse Organisatie voor Wetenschappelijk

Onderzoek (NWO) is acknowledged for providing the computational facilities to run the TM5 model.

References

Andreae M. O. and Merlet, P. (2001). Emission of trace gases and aerosols from biomass burning. *Global Biogeochem. Cycles*, **15** (4), 955–966, doi:110.1029/2000GB001382.

Batenburg, A. M., Walter, S., Pieterse, G., Levin, I., Schmidt, M., Jordan, A., Hammer, S., Yver, C., and Röckmann, T. (2011). Temporal and spatial variability of the stable isotopic composition of atmospheric molecular hydrogen: observations at six EUROHYDROS stations. *Atmos. Chem. Phys.*, **11**, 6985–6999, doi:10.5194/acp–11–6985–2011.

Batenburg, A. M., Schuck, T. J., Baker, A. K., Zahn, A., Brenninkmeijer, C. A. M., and Röckmann, T. (2012). The stable isotopic composition of molecular hydrogen in the tropopause region probed by the CARIBIC aircraft. *Atmos. Chem. Phys.*, **12**(10), 4633–4646, doi:10.5194/acp-12-4633-2012.

Bergamaschi, P., Krol, M., Dentener, F., Vermeulen, A., Meinhardt, F., Graul, R., Ramonet, M., Peters, W., and Dlugokencky, E. J. (2005). Inverse modelling of national and European CH_4 emissions using the atmospheric zoom model TM5. *Atmos. Chem. Phys.*, **5**(9), 2431–2460, 10.5194/acp-5-2431-2005.

Bond, S. W., Vollmer, M. K., Steinbacher, M., Henne, S., and Reimann, S. (2011). Atmospheric molecular hydrogen (H_2): observations at the high-altitude site jungfraujoch, switzerland. *Tellus B*, **63**(1), 64–76, doi: 10.1111/j.1600–0889.2010.00509.x.

Bousquet, P., Hauglustaine, D. A., Peylin, P., Carouge, C., and Ciais, P. (2005). Two decades of OH variability as inferred by an inversion of atmospheric transport and chem-

istry of methyl chloroform. *Atmos. Chem. Phys.*, **5**(10), 2635–2656, doi:10.5194/acp–5–2635–2005.

Bousquet, P., Yver, C., Pison, I., Li, Y. S., Fortems, A., Hauglustaine, D., Szopa, S., Rayner, P. J., Novelli, P., Langenfelds, R., Steele, P., Ramonet, M., Schmidt, M., Foster, P., Morfopoulos, C., and Ciais, P. (2011). A three-dimensional synthesis inversion of the molecular hydrogen cycle: Sources and sinks budget and implications for the soil uptake. *J. Geophys. Res.*, **116**, D01302, doi:10.1029/2010JD014599.

Brenninkmeijer, C. A. M., Crutzen, P., Boumard, F., Dauer, T., Dix, B., Ebinghaus, R., Filippi, D., Fischer, H., Franke, H., Frieβ, U., Heintzenberg, J., Helleis, F., Hermann, M., Kock, H. H., Koeppel, C., Lelieveld, J., Leuenberger, M., Martinsson, B. G., Miemczyk, S., Moret, H. P., Nguyen, H. N., Nyfeler, P., Oram, D., O'Sullivan, D., Penkett, S., Platt, U., Pupek, M., Ramonet, M., Randa, B., Reichelt, M., Rhee, T. S., Rohwer, J., Rosenfeld, K., Scharffe, D., Schlager, H., Schumann, U., Slemr, F., Sprung, D., Stock, P., Thaler, R., Valentino, F., van Velthoven, P., Waibel, A., Wandel, A., Waschitschek, K., Wiedensohler, A., Xueref-Remy, I., Zahn, A., Zech, U., and Ziereis, H. (2007). Civil aircraft for the regular investigation of the atmosphere based on an instrumented container: The new caribic system. *Atmos. Chem. Phys.*, **7**(18), 4953–4976, doi:10.5194/acp–7–4953–2007.

Conrad, R. and Seiler, W. (1980). Contribution of Hydrogen Production by Biological Nitrogen Fixation to the Global Hydrogen Budget. *J. Geophys. Res.*, **85**(C10), 5493–5498, doi:10.1029/JC085iC10p05493.

Conrad, R. and Seiler, W. (1985). Influence of temperature, moisture, and organic carbon on the flux of H_2 and CO between soil and atmosphere: Field studies in subtropical

regions. *J. Geophys. Res.*, **90**(D3), 5699–5709, doi:10.1029/JD090iD03p05699.

Christian, T. J., Kleiss, B., Yokelson, R. J., Holzinger, R., Crutzen, P. J., Hao, W. M., Saharjo, B. H. and Ward, D. E. (2003). Comprehensive laboratory measurements of biomass-burning emissions: 1. emissions from indonesian, african, and other fuels. *J. Geophys. Res.*, **108**, 4719, doi:10.1029/2003JD003704.

Dee, D. P., Uppala, S. M., Simmons, A. J., Berrisford, P., Poli, P., Kobayashi, S., Andrae, U., Balmaseda, M. A., Balsamo, G., Bauer, P., Bechtold, P., Beljaars, A. C. M., van de Berg, L., Bidlot, J., Bormann, N., Delsol, C., Dragani, R., Fuentes, M., Geer, A. J., Haimberger, L., Healy, S. B., Hersbach, H., Hólm, E. V., Isaksen, L., Kållberg, P., Köhler, M., Matricardi, M., McNally, A. P., Monge-Sanz, B. M., Morcrette, J.-J., Park, B.-K., Peubey, C., de Rosnay, P., Tavolato, C., Thépaut, J.-N., and Vitart, F. (2011). The ERA-Interim reanalysis: configuration and performance of the data assimilation system. *Quart. J. R. Meteorol. Soc.*, **137**(656), 553–597, doi:10.1002/qj.828.

EEA (2007). CLC2006 technical guidelines. In *EEA Technical report No.17/2007*. European Environmental Agency.

Ehhalt, D. H. and Rohrer, F. (2009). The tropospheric cycle of H_2: a critical review. *Tellus B*, **61**(3), 500, doi:10.1111/j.1600–0889.2009.00416.x.

Endresen, O., Sø rgard, E., Sundet, J. K., Dalsø ren, S. B., Isaksen, I. S. A., Berglen, T. F. and Gravir, G. (2003). Emissions from international sea transport and environmental impact. *J. Geophys Res.*, **108**(D17), 4560, doi:10.1029/2002JD002898.

Engel, A. and EUROHYDROS PIs (2009). Eurohydros, a european network for atmospheric hydrogen observations and studies. In *EUROHYDROS Final Report*. http://cordis.europa.eu/.

Erickson III, D. J. and Taylor, J. A. (1992). 3-D tropospheric CO modeling - the possible influence of the ocean. *Geophys. Res. Lett.*, **19**(19), 1955–1958, doi:10.1029/92GL01475.

Feck, T., Grooß, J.-U., and Riese, M. (2008). Sensitivity of Arctic ozone loss to stratospheric H_2O. *Geophys. Res. Lett.*, **35**, L01803, doi:10.1029/2007GL031334.

Feilberg, K. L., Johnson, M. S., and Nielsen, C. J. (2004). Relative reaction rates of HCHO, HCDO, DCDO, $H^{13}CHO$, and $HCH^{18}O$ with OH, Cl, Br, and NO_3 radicals. *J. Phys. Chem. A*, **108**, 7393–7398, doi:10.1021/jp048329k.

Foken, T., Meixner, F. X., Falge, E., Zetzsch, C., Serafimovich, A., Bargsten, A., Behrendt, T., Biermann, T., Breuninger, C., Dix, S., Gerken, T., Hunner, M., Lehmann-Pape, L., Hens, K., Jocher, G., Kesselmeier, J., Lüers, J., Mayer, J.-C., Moravek, A., Plake, D., Riederer, M., Rütz, F., Scheibe, M., Siebicke, L., Sörgel, M., Staudt, K., Trebs, I., Tsokankunku, A., Welling, M., Wolff, V., and Zhu, Z. (2012). Coupling processes and exchange of energy and reactive and non-reactive trace gases at a forest site results of the EGER experiment. *Atmos. Chem. Phys.*, **12**(4), 1923–1950, doi:10.5194/acp–12–1923–2012.

Fowler, M., Lowry, D., Fisher, R., Lanoisellé, M., and Nisbet, E. (2011). The long-term (1996-2010) London record of carbon monoxide and molecular hydrogen : evidence for improved air quality. *Geophys. Res. Abstr.*, **13**, 12064–12064.

Francey, R. J., Steele, L. P., Langenfelds, R. L., Lucarelli, M. P., Allison, C. E., Beardsmore, D. J., Coram, S. A., Derek, N., Silva, F. A. d., Etheridge, D. M., Fraser, P. J., Henry, R. J., Turner, B., Welch, E. D., Spencer, D. A., and Cooper, L. N. (1996). Global Atmospheric Sampling Laboratory (GASLAB): supporting and extending the Cape Grim trace gas program. In *Baseline Atmospheric Program Australia 1993*, pages

23–25. Bureau of Meteorology and CSIRO Division of Atmospheric Research, Melbourne.

Ganzeveld, L. N., and Lelieveld J. (1995). Dry deposition parameterization in a chemistry general circulation model and its influence on the distribution of reactive trace gases. *J. Geophys. Res.*, **100**(D10), 20999–21012, doi:10.1029/95JD02266.

Ganzeveld, L. N., Lelieveld, J., and Roelofs, G.-J. (1998). A dry deposition parameterization for sulfur oxides in a chemistry and general circulation model. *J. Geophys Res.*, **105**(D5), 5679–5694, doi:10.1029/97JD03077.

Ganzeveld, L. N., Dentener, F. J., Lelieveld, J., Krol, M. C., and Roelofs, G.-J. (2002). Atmosphere-biosphere trace gas exchanges simulated with a single-column model. *J. Geophys Res.*, **107**(D16), 4297–4317, doi:10.1029/2001JD000684.

Gerst, S. and Quay, P. (2000). The deuterium content of atmospheric molecular hydrogen: Method and initial measurements. *J. Geophys. Res.*, **105**(D21), 26433–26445, doi:10.1029/2000JD900387.

Gerst, S. and Quay, P. (2001). Deuterium component of the global molecular hydrogen cycle. *J. Geophys. Res.*, **106**, 5021–5031, doi:10.1029/2000JD900593.

Gery, M. W., Whitten, G. Z., Killus, J. P., and Dodge, M. C. (1988). Development and testing of the CBM-4 for urban and regional modelling. Technical Report Rep. EPA-600/3-88-012, U.S. Environ. Prot. Agency, Research Triangle Park, N.C.

Gery, M. W., Whitten, G. Z., Killus, J. P., and Dodge, M. C. (1989). A photochemical kinetics mechanism for urban and regional scale computer modeling. *J. Geophys. Res.*, **94**(D10), 12925–12956, doi:10.1029/JD094iD10p12925.

Grant, A., Witham, C. S., Simmonds, P. G., Manning, A. J., and O'Doherty, S. (2010). A 15 year record of high-frequency, in situ measurements of hydrogen at Mace Head, Ireland. *Atmos. Chem. Phys.*, **10**(3), 1203–1214, doi:10.5194/acp–10–1203–2010.

Grooß, J.-U. and Russell III, J. M. (2005). Technical note: A stratospheric climatology for O_3, H_2O, CH_4, NO_x, HCl and HF derived from HALOE measurements. *Atmos. Chem. Phys.*, **5**(10), 2797–2807, doi:10.5194/acp–5–2797–2005.

Hammer, S. and Levin, I. (2009). Seasonal variation of the molecular hydrogen uptake by soils inferred from continuous atmospheric observations in heidelberg, southwest germany. *Tellus B*, **61**, 556–565. doi:10.1111/j.1600–0889.2009.00417.x.

Hauglustaine, D. A. and Ehhalt, D. H. (2002). A three-dimensional model of molecular hydrogen in the troposphere. *J. Geophys. Res.*, **107**(D17), 4330, doi:10.1029/2001JD001156.

Herr, F. L., Scranton, M. I., and Barger, W. R. (1981). Dissolved hydrogen in the Norwegian Sea: Mesoscale surface variability and deep-water distribution. *Deep-Sea Res.*, **28**(9), 1001–1016, doi:10.1016/0198-0149(81)90014-5.

Herr, F. L. (1984). Dissolved hydrogen in Eurasian Arctic waters. *Tellus B*, **36**(1), 55–66, doi:10.1111/j.1600-0889.1984.tb00052.x.

Hooghiemstra, P., Krol, M. C., Bergamaschi, P., de Laat, A. T. J., van der Werf, G. R., Novelli, P. C., Deeter, M. N., Aben, I., and Röckmann, T. (2012). Comparing optimized CO emission estimates using MOPITT or NOAA surface network observations. *J. Geophys. Res.*, **in press**, doi:10.1029/2011JD017043.

Houghton, J. T., Ding, Y., Griggs, D. J., Noguer, M., van der Linden, P. J., Dai, X., Maskell, K., and Johnson, C. A. (2001). *Climate Change 2001: The Scientific Basis.*

Contribution of Working Group I to the Third Assessment Report of the Intergovernmental Panel on Climate Change, chapter 4: Atmospheric Chemistry and Greenhouse Gases. Cambridge University Press, Cambridge, United Kingdom and New York, NY, USA.

Houweling, S., Dentener, F., and Lelieveld, J. (1998). The impact of non-methane hydrocarbon compounds on tropospheric photochemistry. *J. Geophys. Res.*, **103**(D9), 10673–10696, doi:10.1029/97JD03582.

Huijnen, V., Williams, J., van Weele, M., van Noije, T., Krol, M., Dentener, F., Segers, A., Houweling, S., Peters, W., de Laat, J., Boersma, F., Bergamaschi, P., van Velthoven, P., Le Sager, P., Eskes, H., Alkemade, F., Scheele, R., Nédélec, P., and Pätz, H.-W. (2010). The global chemistry transport model TM5: description and evaluation of the tropospheric chemistry version 3.0. *Geosci. Model Dev.*, **3**(2), 445–473, doi:10.5194/gmd–3–445–2010.

Jordan, A. and Steinberg, B. (2011). Calibration of atmospheric hydrogen measurements. *Atmos. Meas. Tech.*, **4**(3), 509–521, doi:10.5194/amt–4–509–2011.

Kopacz, M., Jacob, D. J., Fisher, J. A., Logan, J. A., Zhang, L., Megretskaia, I. A., Yantosca, R. M., Singh, K., Henze, D. K., Burrows, J. P., Buchwitz, M., Khlystova, I., McMillan, W. W., Gille, J. C., Edwards, D. P., Eldering, A., Thouret, V., and Nedelec, P. (2010). Global estimates of CO sources with high resolution by adjoint inversion of multiple satellite datasets (MOPITT, AIRS, SCIAMACHY, TES). *Atmos. Chem. Phys.*, **10**(3), 855–876, doi:10.5194/acp–10–855–2010.

Krol, M., Houweling, S., Bregman, B., van den Broek, M., Segers, A., van Velthoven, P., Peters, W., Dentener, F., and Bergamaschi, P. (2005). The two-way nested global

chemistry-transport zoom model TM5: algorithm and applications. *Atmos. Chem. Phys.*, **5**(2), 417–432, doi:10.5194/acp–5–417–2005.

Langenfelds, R. L., Francey, R. J., Pak, B. C., Steele, L. P., Lloyd, J., Trudinger, C. M., and Allison, C. E. (2002). Interannual growth rate variations of atmospheric CO_2 and its δ^{13}C, H_2, CH_4, and CO between 1992 and 1999 linked to biomass burning. *Global Biogeochem. Cycles*, **16**(3), 1048, doi:10.1029/2001GB001466.

Mar, K. A., McCarthy, M. C., Connell, P., and Boering, K. A. (2007). Modeling the photochemical origins of the extreme deuterium enrichment in stratospheric H_2. *J. Geophys. Res.*, **112**, D19302, doi:10.1029/2006JD007403.

McCarthy, M. C., Boering, K. A., Rahn, T., Eiler, J., Rice, A., Tyler, S. C., and Atlas, E. (2004). The hydrogen isotopic composition of water vapor entering the stratosphere inferred from high precision measurements of δD-CH_4 and δD-H_2. *J. Geophys Res.*, **109**, D07304, doi:10.1029/2003JD004003.

Meirink, J. F., Bergamaschi, P., Frankenberg, C., dAmelio, M. T. S., Dlugokencky, E. J., Gatti, L. V., Houweling, S., Miller, J. B., Röckmann, T., Villani, M. G., and Krol, M. C. (2008a). Four-dimensional variational data assimilation for inverse modelling of atmospheric methane emissions: Analysis of SCIAMACHY observations. *J. Geophys. Res.*, **113**, D17301, doi:10.1029/2007JD009740.

Meirink, J. F., Bergamaschi, P., and Krol, M. C. (2008b). Four-dimensional variational data assimilation for inverse modelling of atmospheric methane emissions: method and comparison with synthesis inversion. *Atmos. Chem. Phys.*, **8**(21), 6341–6353, doi:10.5194/acp–8–6341–2008.

Müller, J.-F. (1992). Geographical distribution and seasonal variation of surface emissions and deposition velocities of atmospheric trace gases. *J. Geophys. Res.*, **97**(D4), 3787–3804, doi:10.1029/91JD02757.

Nilsson, E. J. K., Andersen, V. F., Skov, H., and Johnson, M. S. (2010). Pressure dependent deuterium fractionation in the formation of molecular hydrogen in formaldehyde photolysis. *Atmos. Chem. Phys.*, **10**, 3455–3462, doi:10.5194/acp–10–3455–2010.

Noije, T. P. C. van, Eskes, H. J., Weele, M. van, and Velthoven, P. F. J. van (2004). Implications of the enhanced Brewer-Dobson circulation in European Centre for Medium-Range Weather Forecasts reanalysis ERA-40 for the stratosphere-troposphere exchange of ozone in global chemistry transport models. *J. Geophys. Res.*, **109**, D19308, doi:10.1029/2004JD004586.

Novelli, P. C., Lang, P. M., Masarie, K. A., Hurst, D. F., Myers, R., and Elkins, J. W. (1999). Molecular hydrogen in the troposphere: Global distribution and budget. *J. Geophys. Res.*, **104**(D23), 30427–30444, doi:10.1029/1999JD900788.

Patra, P. K., Law, R. M., Peters, W., Rödenbeck, C., Takigawa, M., Aulagnier, C., Baker, I., Bergmann, D. J., Bousquet, P., Brandt, J., Bruhwiler, L., Cameron-Smith, P. J., Christensen, J. H., Delage, F., Denning, A. S., Fan, S., Geels, C., Houweling, S., Imasu, R., Karstens, U., Kawa, S. R., Kleist, J., Krol, M. C., Lin, S.-J., Lokupitiya, R., Maki, T., Maksyutov, S., Niwa, Y., Onishi, R., Parazoo, N., Pieterse, G., Rivier, L., Satoh, M., Serrar, S., Taguchi, S., Vautard, R., Vermeulen, A. T., and Zhu, Z. (2008). TransCom model simulations of hourly atmospheric CO_2: Analysis of synoptic-scale variations for the period 2002-2003. *Glob. Biogeochem. Cycl.*, **22**, GB4013, doi:10.1029/2007GB003081.

Pieterse, G., Krol, M. C., and Röckmann, T. (2009). A consistent molecular hydrogen isotope chemistry scheme based on an independent bond approximation. *Atmos. Chem. Phys.*, **9**, 8503–8529, doi:10.5194/acp–9–8503–2009.

Pieterse, G., Krol, M. C., Batenburg, A. M., Steele, L. P., Krummel, P. B., Langenfelds, R. L., and Röckmann, T. (2011). Global modelling of H_2 mixing ratios and isotopic compositions with the TM5 model. *Atmos. Chem. Phys.*, **11**(14), 7001–7026, doi:10.5194/acp–11–7001–2011.

Pison, I., Bousquet, P., Chevallier, F., Szopa, S., and Hauglustaine, D. (2009). Multi-species inversion of CH_4, CO and H_2 emissions from surface measurements. *Atmos. Chem. Phys.*, **9**(14), 5281–5297, doi:10.5194/acp–9–5281–2009.

Popa, M. E., Vermeulen, A. T., van den Bulk, W. C. M., Jongejan, P. A. C., Batenburg, A. M., Zahorowski, W., and Röckmann, T. (2011). H_2 vertical profiles in the continental boundary layer: measurements at the Cabauw tall tower in The Netherlands. *Atmos. Chem. Phys.*, **11**(13), 6425–6443, doi:10.5194/acp–11–6425–2011.

Price, H., Jaeglé, L., Rice, A., Quay, P., Novelli, P. C., and R., G. (2007). Global budget of molecular hydrogen and its deuterium content: Constraints from ground station, cruise, and aircraft observations. *J. Geophys. Res.*, **112**, D22108, doi:10.1029/2006JD008152.

Pul, W. A. J. van, and Jacobs, A. F. G. (1994). The conductance of a maize crop and the underlying soil to ozone under various environmental conditions. *Bound.-Lay. Meteorol.*, **69**(1), 83–99, doi:10.1007/BF00713296.

Rahn, T., Kitchen, N., and Eiler, J. M. (2002). D/H ratios of atmospheric H_2 in urban air: Results using new methods for analysis of nano-molar H_2 samples. *Geochim. Cosmochim. Acta*, **66**, 2475–2481, doi:10.1016/S0016–7037(02)00858–X.

Rahn, T., Eiler, J. M., Boering, K. A., Wennberg, P. O., McCarthy, M. C., Tyler, S., Schauffler, S., Donnelly, S., and Atlas, E. (2003). Extreme deuterium enrichment in stratospheric hydrogen and the global atmospheric budget of H_2. *Nature*, **424**, 918–921, doi:10.1038/nature01917.

Rhee, T. S., Mak, J. E., Brenninkmeijer, C. A. M., and Röckmann, T. (2004). Continuous-flow isotope analysis of the D/H ratio in atmospheric hydrogen. *Rap. Commun. Mass Spectrom.*, **18**, 299–306, doi:10.1002/rcm.1309.

Rhee, T. S., Brenninkmeijer, C. A. M., and Röckmann, T. (2006). The overwhelming role of soils in the global atmospheric hydrogen cycle. *Atmos. Chem. Phys.*, **6**, 1611–1625, doi:10.5194/acp–6–1611–2006.

Rice, A., Quay, P., Stutsman, J., Gammon, R., Price, H., and Jaeglé, L. (2010). Meridional distribution of molecular hydrogen and its deuterium content in the atmosphere. *J. Geophys. Res.*, **115**, D12306, doi:10.1029/2009JD012529.

Röckmann, T., Rhee, T. S., and Engel, A. (2003). Heavy hydrogen in the stratosphere. *Atmos. Chem. Phys.*, **3**, 2015–2023, doi:10.5194/acp–3–2015–2003.

Röckmann, T., Walter, S., Bohn, B., Wegener, R., Spahn, H., Brauers, T., Tillmann, R., Schlosser, E., Koppmann, R., and Rohrer, F. (2010). Isotope effect in the formation of H_2 from H_2CO studied at the atmospheric simulation chamber SAPHIR. *Atmos. Chem. Phys.*, **10**, 5343–5357, doi:10.5194/acp–10–5343–2010.

Sander, S. P., Finlayson-Pitts, B. J., Friedl, R. R., Golden, D. M., Huie, R. E., Keller-Rudek, H., Kolb, C. E., Kurylo, M. J., Molina, M. J., Moortgat, G. K., Orkin, V. L., R., R. A., and Wine, P. H. (2006). Chemical kinetics and photochemical data for use in atmospheric studies, evaluation number 15. Technical report, JPL Publication 06-2,

Jet Propulsion Laboratory, Pasadena.

Sanderson, M. G., Collins, W. J., Derwent, R. G., and Johnson, C. E. (2003). Simulation of global hydrogen levels using a lagrangian three dimensional model. *J. Atmos. Chem.*, **46**(1), 15–28, doi:10.1023/A:1024824223232.

Schaap, M., Roemer, M., Sauter, F., Boersen, G., Timmermans, R., Vermeulen, A. T., and Builtjens, P. J. H. (2005). LOTOS-EUROS: Documentation. Technical report, Netherlands Organisation for Applied Scientific Research (TNO), Apeldoorn, The Netherlands.

Schultz, M. G. and Stein, O. (2006). GEMS (GRG) emissions for 2003 reanalysis simulations. Technical report, MPI-M.

Schultz, M. G., Diehl, T., Brasseur, G. P., and Zittel, W. (2003). Air pollution and climate-forcing impacts of a global hydrogen economy. *Science*, **302**(5645), 624–627, doi:10.1126/science.1089527.

Schultz, M. G., Backman, L., Balkanski, Y., Bjoerndalsaeter, S., Brand, R., Burrows, J. P., Dalsoeren, S., Vasconcelos, M. de, Grodtmann, B., Hauglustaine, D. A., Heil, A., Hoelzemann, J. J., Isaksen, I. S. A., Kaurola, J., Knorr, W., Ladstaetter-Weißenmayer, A., Mota, B., Oom, D., Pacyna, J., Panasiuk, D., Pereira, J. M. C., Pulles, T., Pyle, J., Rast, S., Richter, A., Savage, N., Schnadt, C., Schulz, M., Spessa, A., Staehelin, J., Sundet, J. K., Szopa, S., Thonicke, K., Bolscher, M. van het, Noije, T. van, Velthoven, P. van, Vik, A. F., and Wittrock, F. (2007). REanalysis of the TROpospheric chemical composition over the past 40 years (RETRO) – a long-term global modeling study of tropospheric chemistry. Technical report, Max Planck Institute for Meteorology, Jülich/Hamburg, Germany.

Tromp, T. K., Shia, R.-L., Allen, M., Eiler, J. M., and Yung, Y. L. (2003). Potential environmental impact of a hydrogen economy on the stratosphere. *Science*, **300**(5626), 1740–1742, doi:10.1126/science.1085169.

Villani, M. G., Bergamaschi, P., Krol, M. C., Meirink, J. F., and Dentener, F. (2010). Inverse modeling of European CH4 emissions: sensitivity to the observational network. *Atmos. Chem. Phys.*, **10**, 1249–1267, doi:10.5194/acp–10–1249–2010.

Vogel, B., Feck, T., Grooß, J.-U., and Riese, M. (2012). Impact of a possible future global hydrogen economy on arctic stratospheric ozone loss. *Energy Environ. Sci.*, **5**(4), 6445–6452, doi:10.1039/C2EE03181G.

Vollmer, M. K., Walter, S., Mohn, J., Steinbacher, M., Bond, S. W., Röckmann, T., and Reimann, S. (2012). Molecular hydrogen (H_2) combustion emissions and their isotope (D/H) signatures from domestic heaters, diesel vehicle engines, waste incinerator plants, and biomass burning. *Atmos. Chem. Phys. Discuss.*, **12**(3), 6839–6875, doi:10.5194/acpd–12–6839–2012.

Warwick, N. J., Bekki, S., Nisbet, E. G., and Pyle, J. A. (2004). Impact of a hydrogen economy on the stratosphere and troposphere studied in a 2D model. *Geophys. Res. Lett.*, **31**, L05107, doi:10.1029/2003GL019224.

Werf, G. R. van der, Randerson, J. T., Collatz, G. J. and Giglio., L. (2003). Carbon emissions from fires in tropical and subtropical ecosystems. *Glob. Change Biol.*, **9**, 547–562, doi:10.1046/j.1365–2486.2003.00604.x.

Werf, G. R. van der, Randerson, J. T., Giglio, L. , Collatz, G. J., Mu, M., Kasibhatla, P. S., Morton, D. C., DeFries, R. S., Jin, Y., and Leeuwen, T. T. van (2010). Global fire emissions and the contribution of deforestation, savanna, forest, agricultural, and

peat fires (1997-2009). *Atmos. Chem. Phys.*, **10**(23), 11707–11735, doi:10.5194/acp–10–11707–2010.

Xiao, X., Prinn, R. G., Simmonds, P. G., Steele, L. P., Novelli, P. C., Huang, J., Langenfelds, R. L., O'Doherty, S., Krummel, P. B., Fraser, P. J., Porter, L. W., Weiss, R. F., Salameh, P., and Wang, R. H. J. (2007). Optimal estimation of the soil uptake of molecular hydrogen from the advanced global atmospheric gases experiments and other measurements. *J. Geophys. Res.*, **112**, D07303, doi:10.1029/2006JD007241.

Yashiro, H., Sudo, K., Yonemura, S., and Takigawa, M. (2011). The impact of soil uptake on the global distribution of molecular hydrogen: chemical transport model simulation. *Atmos. Chem. Phys.*, **11**, 6701–6719, doi:10.5194/acp–11–6701–2011.

Yonemura, S., Kawashima, S., and Tsuruta, H. (2000). Carbon monoxide, hydrogen, and methane uptake by soils in a temperate arable field and a forest. *J. Geophys. Res.*, **105**(D11), 14347–14362, doi:10.1029/1999JD901156.

Yver, C., Schmidt, M., Bousquet, P., Zahorowski, W., and Ramonet, M. (2009). Estimation of the molecular hydrogen soil uptake and traffic emissions at a suburban site near Paris through hydrogen, carbon monoxide, and radon-222 semicontinuous measurements. *J. Geophys. Res.*, **114**, D18304, doi:10.1029/2009JD012122.

Yver, C. E., Pison, I. C., Fortems-Cheiney, A., Schmidt, M., Chevallier, F., Ramonet, M., Jordan, A., Søvde, O. A., Engel, A., Fisher, R. E., Lowry, D., Nisbet, E. G., Levin, I., Hammer, S., Necki, J., Bartyzel, J., Reimann, S., Vollmer, M. K., Steinbacher, M., Aalto, T., Maione, M., Arduini, J., O'Doherty, S., Grant, A., Sturges, W. T., Forster, G. L., Lunder, C. R., Privalov, V., Paramonova, N., Werner, A., and Bousquet, P. (2011). A new estimation of the recent tropospheric molecular hydrogen budget using

atmospheric observations and variational inversion. *Atmos. Chem. Phys.*, **11**(7), 3375–3392, doi:10.5194/acp–11–3375–2011.

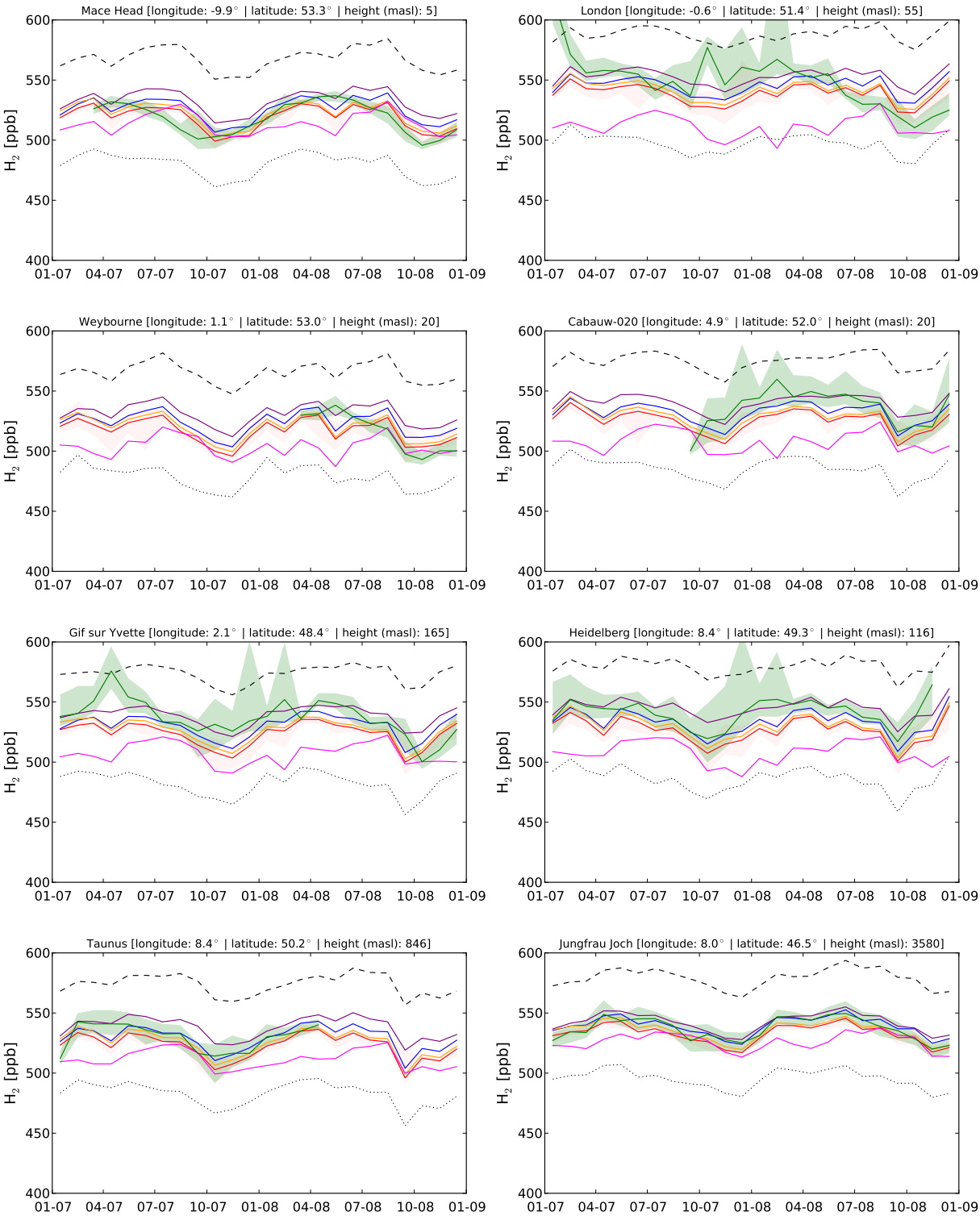

Figure 1. Comparison of modelled monthly median H_2 mixing ratios with available measurements from the EuroHydros project. The green lines represent the observational data. The following model scenarios are shown: **S1 (dotted), S2 (dashed), S3a (blue), S3b (orange), S3c (red), S4 (magenta) and S6 (purple)**. The shaded areas indicate the lower and upper quartile of the variability in the measurements and model results. Dates on the x-axis are shown in MM-YY format.

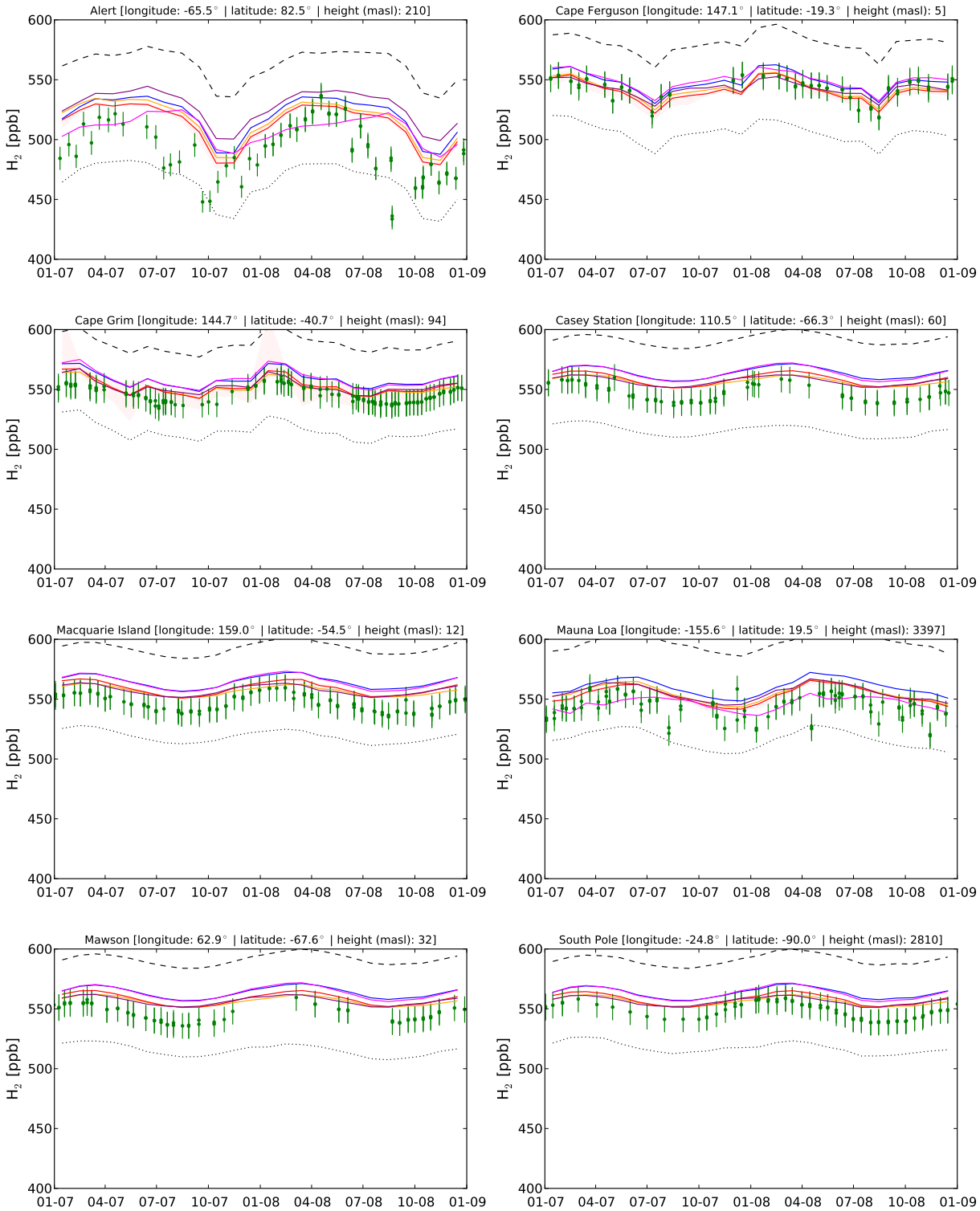

Figure 2. Comparison of modelled monthly median H_2 mixing ratios with available measurements from the flask sampling CSIRO network. The circles represent the event samples. The following model scenarios are shown: **S1 (dotted), S2 (dashed), S3a (blue), S3b (orange), S3c (red), S4 (magenta) and S6 (purple)**. The shaded areas indicate the lower and upper quartile of the variability in the model results. Dates on the x-axis are shown in MM-YY format.

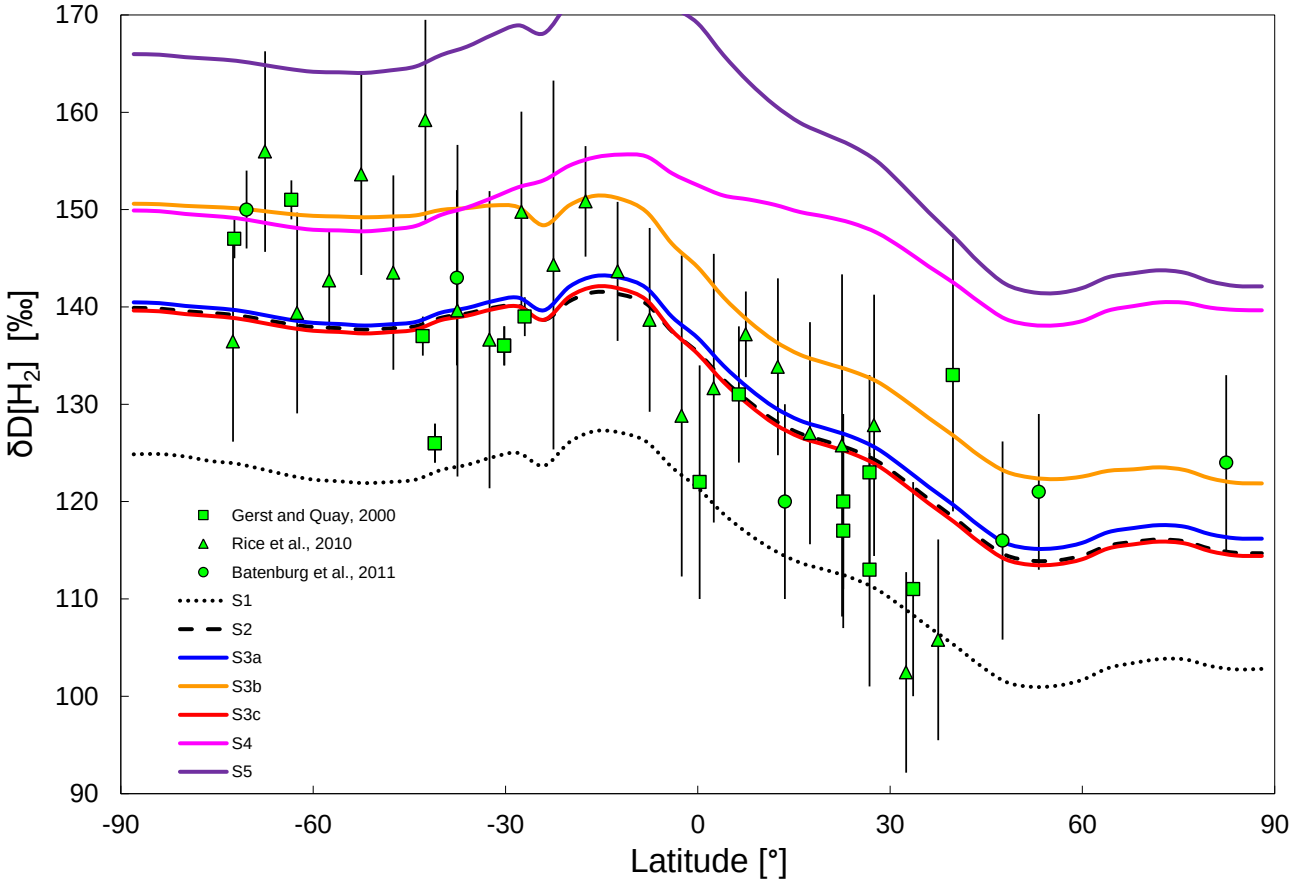

Figure 3. Comparison of the modelled **free oceanic** latitudinal gradient of $\delta D\,[H_2]$ ~~in marine air~~ with available measurement data. The green squares represent data points from Gerst and Quay [2000], the green triangles represent data points from Rice *et al.* [2010], and the green circles represent data points from the EuroHydros project [Batenburg *et al.*, 2011]. The following model scenarios are shown: **S1 (dotted), S2 (dashed), S3a (blue), S3b (orange), S3c (red), S4 (magenta) and S6 (purple)**. ~~The latter two~~**Scenario S2-S6** use the **updated** stratospheric parametrisation derived from the CARIBIC measurements [Batenburg *et al.*, 2012] as upper boundary condition.

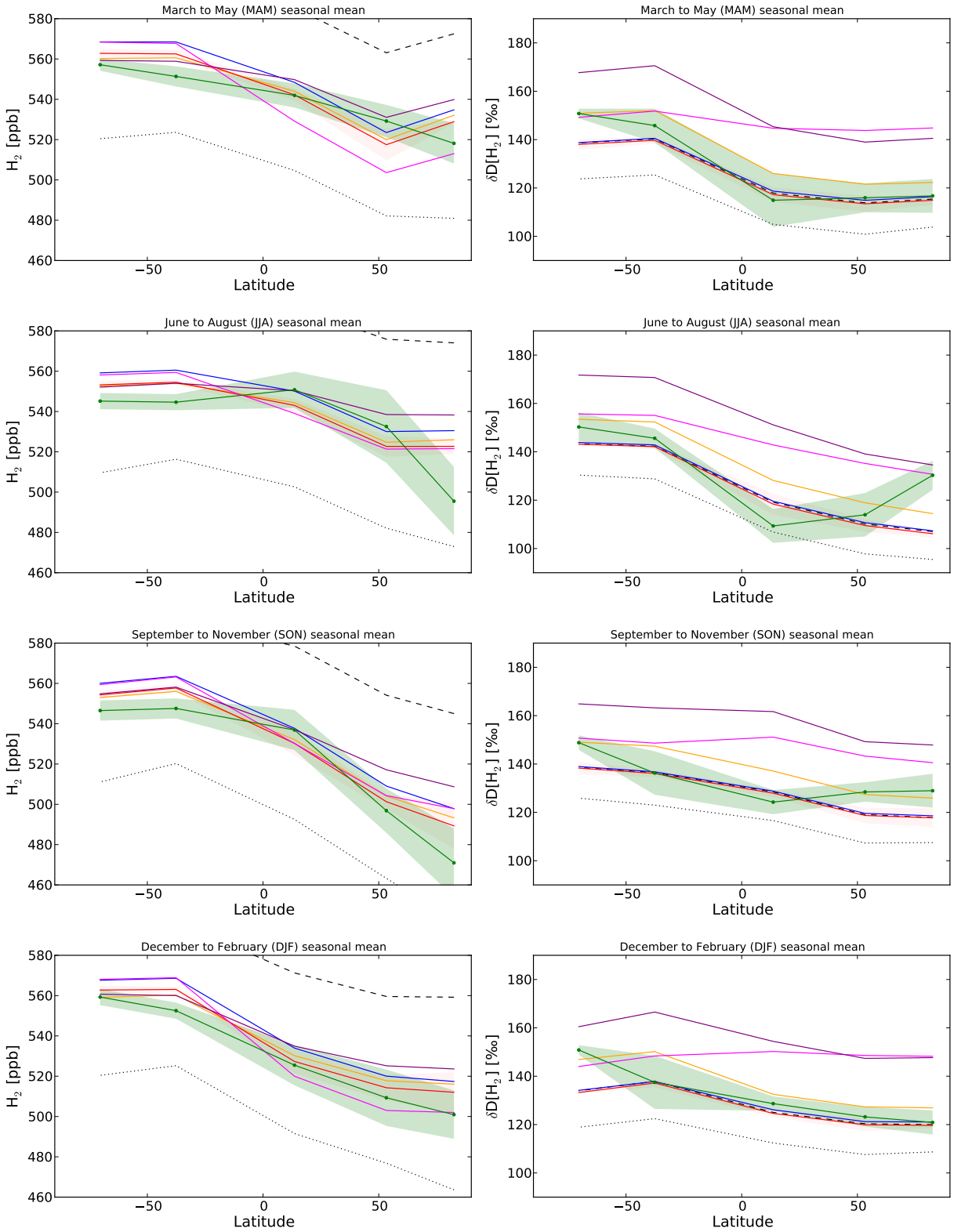

Figure 4. Comparison of the modelled seasonal mean latitudinal gradients of the H_2 mixing ratio (left) and isotopic composition (right) with available measurement data (green) from the EuroHydros project [Batenburg *et al.*, 2011]. The shaded areas indicate the within-season standard deviations of the measurements and model results. The following model scenarios are shown: S1 (dotted), S2 (dashed), S3a (blue), S3b (orange), S3c (red), S4 (magenta) and S6 (purple). Scenario S2-S6 use the updated stratospheric parametrisation derived from the CARIBIC measurements [Batenburg *et al.*, 2012] as upper boundary condition.

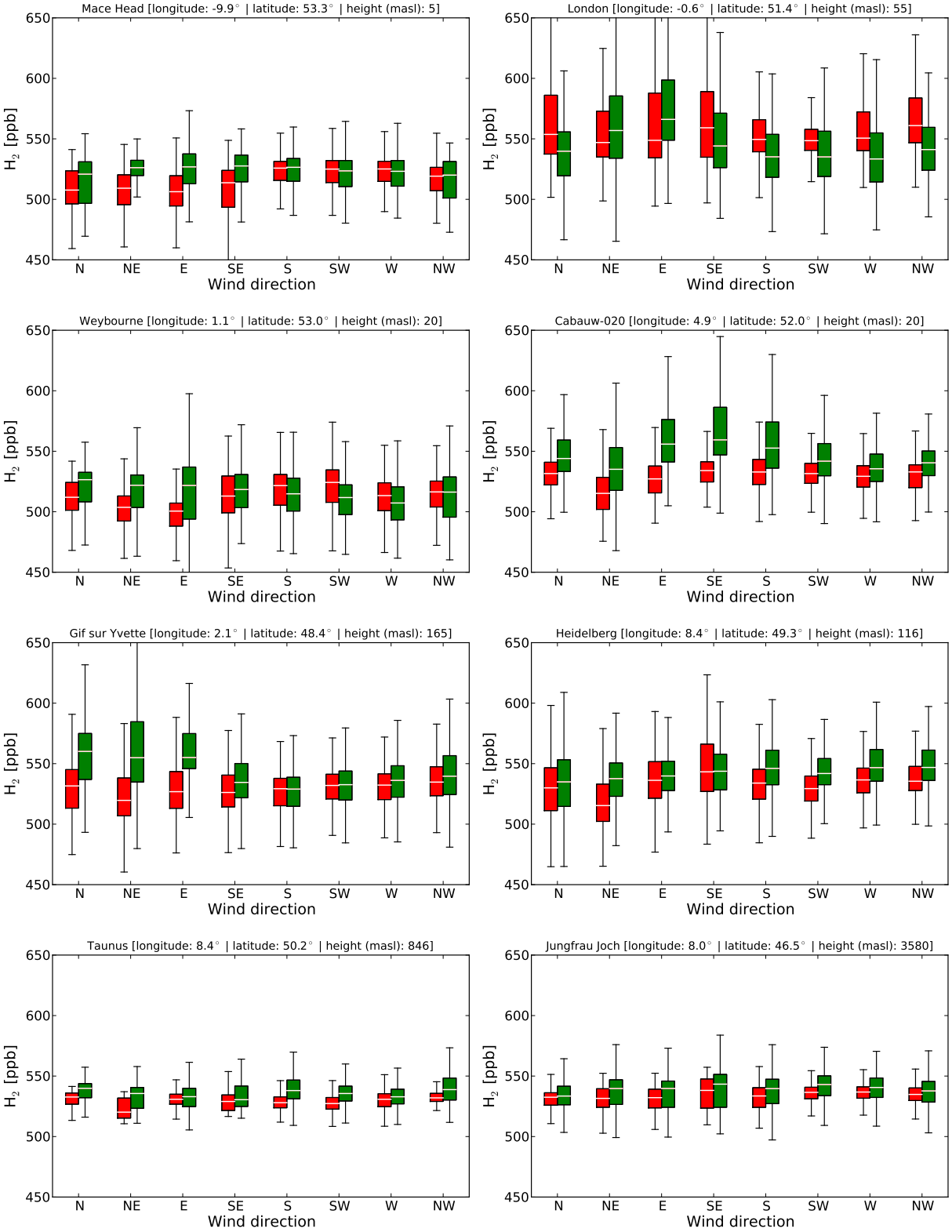

Figure 5. **Comparison of modelled H_2 mixing ratios obtained with scenario S3c with available measurement data (green) from the EuroHydros project, aggregated per wind sector. The median values are shown as white horizontal lines in the boxes that show the upper and lower quartiles. The 5 and 95 percentiles are indicated by the whiskers.**

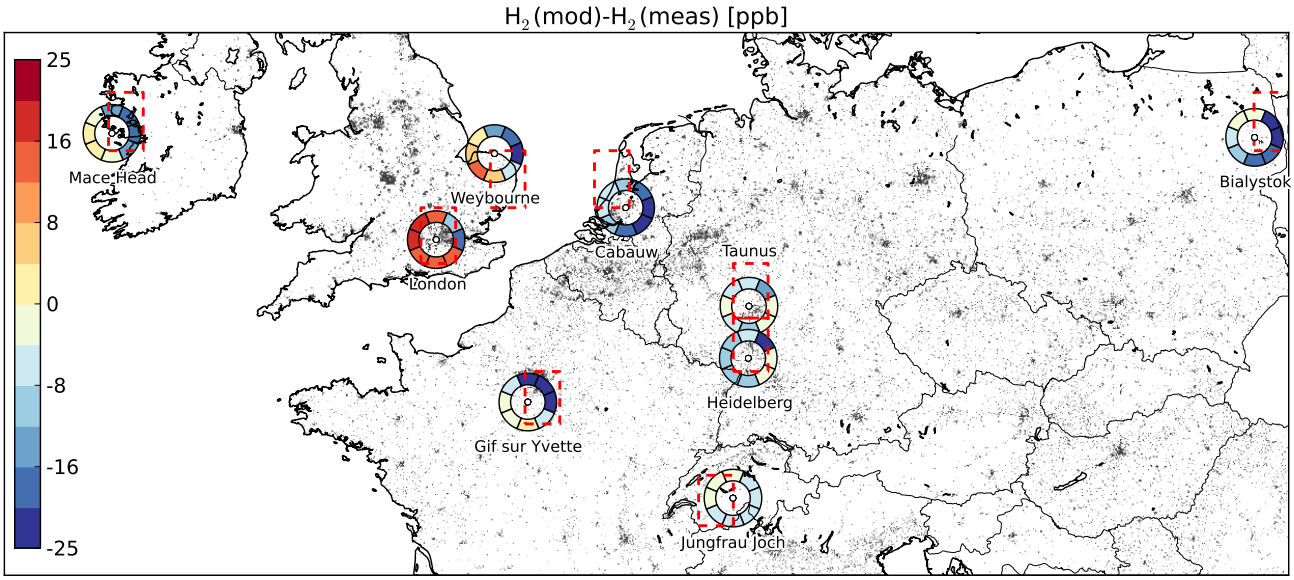

Figure 6. Overview of the difference between the modelled and measured H_2 median mixing ratios of ~~the reduced deposition~~ scenario **S3c**~~(top) and increased fossil fuel emission scenario (bottom)~~, calculated per wind sector and shown as a coloured wind rose around the location of each station (white circle). Urban areas shown in grey were obtained from the Corine Land Cover (CLC) 2006 database [EEA, 2007]. The 1 by 1 degree grid cells that belong to each station are shown as dashed red squares.

Table 1. Overview of scenarios aiming at closing the global budget of H_2 and $\delta D\,[H_2]$.

Name	Explanation	Change in Budget term[a]	Change in Burden[b]
S1	Different meteorology[c]	-	−1.9%
S2	Corrected deposition parametrisation	-	+12.1%
S3a	Reduced in-canopy deposition resistance	+16.8%	+6.4%
S3b	Reduced in-canopy deposition resistance +	+15.7%	+5.1%
	Decreased ocean N_2 fixation emissions	−40.0%	
S3c	Adjusted deposition[d]	+20.2%	+5.1%
S4	Decreased fossil fuel burning emissions	−81.3%	+5.1%
S5	Increased photochemical removal	+39.2%	+5.1%

[a] This is the observed relative change in the corresponding budget term compared to scenario S2, see Table 3.
[b] The changes in the burden for scenario S1 and S2 are calculated relative to the burden of 157 Tg H_2/yr reported in Pieterse *et al.* [2011].
[c] This is the unchanged implementation of the model described by Pieterse *et al.* [2011] driven by ERA-Interim meteorology.
[d] In order to reduce the inter-hemispheric gradient observed in S3a, the original soil deposition velocities reported by Sanderson *et al.* [2003] above forests and Savannah ecosystem types were increased by 10% and the deposition velocities to agricultural regions were decreased by 10%. As a result the SH H_2 mixing ratios decrease, whereas the NH mixing ratios remain more or less the same.

Table 2. Overview of $\tilde{\chi}^2$–values[a] for different model scenarios for H_2 and $\delta D\,[H_2]$.

	Sampling method	Parameter	n	$\tilde{\chi}^2$						
				S1	S2	S3a	S3b	S3c	S4	S5
Performance per comparison study										
Section 3.1, EuroHydros data	noon-time[b]	H_2	10426	4.5	2.3	0.9	1.0	1.1	2.9	0.8
Section 3.1, CSIRO data	event	H_2	663	4.5	9.7	1.6	1.0	1.0	1.3	1.4
Section 3.2, Mean latitudinal gradient	[c]	$\delta D\,[H_2]$	48	1.5	0.4	0.4	0.8	0.4	1.7	4.3
Section 3.2, Seasonal latitudinal gradient	event	$\delta D\,[H_2]$	321	3.0	0.9	0.9	0.8	1.0	3.9	5.1
Section 3.2, Seasonal latitudinal gradient	event	H_2	382	6.8	12.1	1.7	1.2	1.1	1.5	2.3
Section 3.3, EuroHydros data	continuous	H_2	72026	5.9	4.7	1.1	1.1	1.2	3.7	1.2
Section 3.3, EuroHydros data (w/o London)	continuous	H_2	63392	6.4	4.7	1.0	1.0	1.1	3.5	1.0
Overall performance for H_2										
			83497	5.8	4.5	1.1	1.1	1.2	3.6	1.1
Overall performance for $\delta D\,[H_2]$										
			369	2.8	0.9	0.9	0.8	0.9	3.6	5.0

[a] See Equation 10 in Section 2.4.
[b] The local noon-time model results were sampled for this comparison, see Section 2.4.
[c] Most measurement data were obtained during ship cruises on the Atlantic and Pacific Ocean. Furthermore, exact sampling times were not available for all data. Therefore, model data above the free Atlantic and Pacific Ocean (far away from the land masses) were selected to calculate an overall annual mean latitudinal gradient. Subsequently, the model values for the different stations were obtained by interpolation to the different station latitudes.

Table 3. Global budget of H_2 for the year 2008 compared to existing budgets (numbers in Tg H_2/yr).

	Novelli et al. (1999)	Rhee et al. (2006)	Xiao et al. (2007)	Ehhalt and Rohrer (2009)	Pieterse et al. (2011)	Scenarios in this work						
						S1	S2	S3a	S3b	S3c	S4	S5
Sources												
Fossil fuel	15±**10**	15±**6**	15±**10**	11±**4**	17.0	17.1	17.1	17.1	17.1	17.1	3.2	17.1
Biomass burning	16±**5**	16±**3**	13±**3**	15±**6**	15.0	15.0	15.0	15.0	15.0	15.0	15.0	15.0
Biofuel												
Ocean N_2 fixation	3±**2**	6±**5**		6±**3**	5.0	5.0	5.0	5.0	3.0	5.0	5.0	5.0
Land N_2 fixation	3±**1**	6±**5**		3±**2**	3.0	3.0	3.0	3.0	3.0	3.0	3.0	3.0
Photochemical production	40±**16**	64±**12**	77±**10**	41±**11**	37.3	36.9	36.8	36.9	36.9	36.9	36.9	36.4
Vertical flux[a]					-0.1	0.3	-0.3	0.0	0.1	0.1	0.1	0.1
Stratospheric correction flux[b]					0.4	2.4	-7.5	-2.1	-1.2	-1.1	-0.9	-1.1
Total	77±**16**	107±**15**	105±**10**	76±**14**	77.6	79.7	69.1	74.9	73.9	76.0	62.3	75.5
Sinks												
Photochemical removal	19±**5**	19±**3**	18±**3**	19±**5**	22.1	21.3	24.5	23.1	22.8	22.8	22.8	34.1
Deposition	56±**41**	88±**11**	85±**5**	60^{+30}_{-20}	55.8	58.4	44.0	51.4	50.9	52.9	39.5	41.2
Total	75±**41**	107±**11**	105[c]	79^{+30}_{-20}	77.9	79.7	68.5	74.5	73.7	75.7	62.3	75.3
Overall												
Tropospheric burden (Tg H_2)	155±**10**	150[d]	149±**23**	155[e]±**10**	157[f]	154[f]	176[f]	167[f]	165[f]	165[f]	165[f]	165[f]
Tropospheric lifetime (yr)	2.1	1.4	1.4	2.0	2.0[f]	1.9[f]	2.6[f]	2.3[f]	2.2[f]	2.2[f]	2.7[f]	2.2[f]
Isotopic composition (‰)[g]					128	128	144	139	144	139	155	167
Stratospheric correction (‰)[g]					29	59	-137	-22	-16	0	-32	-53

[a] This term accounts for the influx of H_2 from the stratospheric model levels below 100 hPa.
[b] This term accounts for the stratospheric correction (see Section 2.5) for the part of the stratosphere that is in the model domain down to 100 hPa.
[c] Includes export to stratosphere of 1.9 Tg H_2 per year.
[d] Calculated from sources and lifetime.
[e] From Novelli *et al.* [1999].
[f] The values in the table are calculated from the burden and lifetimes of H_2 in the model domain from the surface down to 100 hPa by assuming that 92.3% of the mass in this domain resides in the troposphere.
[g] The stratospheric correction is part of the overall value for the isotopic composition relative to VSMOW down to 100 hPa.